Struct Multidisc Optim (2011) 43:419–442
DOI 10.1007/s00158-010-0568-9

RESEARCH PAPER

# Adaptive-sparse polynomial chaos expansion for reliability analysis and design of complex engineering systems

**Chao Hu · Byeng D. Youn**

Received: 30 October 2009 / Revised: 8 August 2010 / Accepted: 14 August 2010 / Published online: 23 September 2010


**Abstract** This paper presents an adaptive-sparse polynomial chaos expansion (adaptive-sparse PCE) method for performing engineering reliability analysis and design. The proposed method combines three ideas: (i) an adaptive-sparse scheme to build sparse PCE with the minimum number of bivariate basis functions, (ii) a new projection method using dimension reduction techniques to effectively compute the expansion coefficients of system responses, and (iii) an integration of copula to handle nonlinear correlation of input random variables. The proposed method thus has three positive features for reliability analysis and design: (a) there is no need for response sensitivity analysis, (b) it is highly efficient and accurate for reliability analysis and its sensitivity analysis, and (c) it is capable of handling a nonlinear correlation. In addition to the features, an error decomposition scheme for the proposed method is presented to help analyze error sources in probability analysis. Several engineering problems are used to demonstrate the three positive features of the adaptive-sparse PCE method.

**Keywords** Polynomial chaos expansion · Dimension reduction · Reliability analysis · RBRDO · Copula

C. Hu
Department of Mechanical Engineering,
University of Maryland at College Park,
College Park, MD 20742, USA

B. D. Youn (✉)
School of Mechanical and Aerospace Engineering,
Seoul National University,
301-1520 Gwanak-ro 599, Gwanak-gu,
Seoul, 151-742, South Korea
e-mail: bdyoun@snu.ac.kr

## 1 Introduction

Reliability analysis is an essential part of engineering product and process development. Various methods have been developed to assess engineering product reliability and process quality while taking into account different variability sources (e.g., material properties, loads, geometric tolerances). In order to formulate reliability analysis in a mathematical framework, random variables are often used to model variability sources in product and process developments. Reliability analysis can then be formulated as a multi-dimensional integration over a safety domain as

$$R = \int_{\Omega^S} f(\mathbf{x}) d\mathbf{x} \tag{1}$$

where $R$ denotes the product reliability; $f(\mathbf{x})$ denotes the joint probability density function (PDF) of the vector of random variables; $\mathbf{x} = (x_1, x_2, ..., x_N)^{\mathrm{T}}$ models variability sources such as material properties, loads, geometric tolerances; the safety domain $\Omega^{\mathrm{S}}$ is defined by the limit-state function as $\Omega^{\mathrm{S}} = \{\mathbf{x}\colon g(\mathbf{x}) < 0\}$; $g(\mathbf{x})$ is a product performance function.

In practice, however, it is extremely difficult to perform the multi-dimensional numerical integration when the number of random variables is relatively large. The search for efficient computational procedures to estimate reliability has resulted in a variety of numerical and simulation methods, such as the first- or second-order reliability method (FORM/SORM) (Hasofer and Lind 1974; Breitung 1984; Tvedt 1984; Youn and Choi 2004a; Wang and Grandhi 1996), direct or smart Monte Carlo simulation (MCS) (Rubinstein 1981; Fu and Moses 1988; Au and Beck 2001), the dimension reduction (DR) method (Rahman and Xu 2004; Xu and Rahman 2004; Youn et al. 2007a), and the stochastic spectral method (Ghanem and Spanos

1991; Paffrath and Wever 2007, Wiener 1938; Xiu and Karniadakis 2003).

Among the many reliability analysis methods, the first- or second-order reliability method (FORM or SORM) is most commonly used. The FORM/SORM uses the first- or second-order Taylor expansion to approximate a limit-state function at the most probable failure point (MPP) where the limit-state function separates failure and safety regions of a product (or process) response. Some major challenges of the FORM/SORM are that (i) it is very expensive to build the probability density function (PDF) of the response and (ii) the product/process design can also be expensive when employing a large number of the responses. Direct or smart MCS provides an alternative means of multi-dimensional integration (Rubinstein 1981; Fu and Moses 1988; Au and Beck 2001). Although MCS produces accurate results for reliability analysis, it demands a prohibitively large number of simulation runs. Thus, it is often used merely as a benchmark in reliability analysis.

Recently, the dimension reduction (DR) method (Rahman and Xu 2004; Xu and Rahman 2004) has been proposed and has been shown to be a sensitivity-free method for reliability analysis. This method uses an additive decomposition of a response that simplifies a single multi-dimensional integration to multiple one-dimensional integrations by the univariate DR (UDR) method (Rahman and Xu 2004) or to multiple one- and two-dimensional integrations by the bivariate DR (BDR) method (Xu and Rahman 2004). Recently, the eigenvector dimension reduction (EDR) method (Youn et al. 2007a) has improved the numerical efficiency and stability of the UDR method with the ideas of eigenvector samples and stepwise moving least squares method with no extra expense. Results of the DR-family methods are given in the form of statistical moments. To further predict the reliability or PDF of the response, PDF-generation techniques must be involved, which could slightly increase numerical error in reliability prediction.

The stochastic spectral method (Ghanem and Spanos 1991) is an emerging technique for reliability analysis of complex engineering problems. This method uses a number of response samples and generates a stochastic response surface approximation with multi-dimensional polynomials over a sample space of random variables. Once the explicit response surface is constructed, MCS is often used for reliability analysis due to its convenience. The most popular stochastic spectral method is the polynomial chaos expansion (PCE) method. The original Hermite polynomial chaos basis was proposed by Wiener (1938) for modeling stochastic responses with Gaussian input random variables. Xiu and Karniadakis (2003) extended the method under the Askey polynomial scheme to non-Gaussian random variables (e.g., gamma, uniform, and beta), referred to as the generalized PCE. The wavelet basis (Le Maitre et al. 2004) and multi-element generalized PCE (Wan and Karniadakis 2006) were developed to further extend the generalized PCE to use the polynomial basis functions that are not globally smooth. For the estimation of small failure probability, shifted and windowed Hermite polynomial chaos were proposed to enhance the accuracy of a response surface in the failure region (Paffrath and Wever 2007). In recent papers (Sudret and Der Kiureghian 2002; Choi et al. 2004a, b; Blatman and Sudret 2008), researchers have applied this method to various engineering reliability problems. Although the PCE method is considered to be accurate, the primary drawback of the PCE method is the curse of dimensionality, which substantially increases the computational cost as the number of random variables increases. To alleviate the difficulty, many adaptive algorithms were recently developed. The authors in Wan and Karniadakis (2005) proposed an adaptive multi-element generalized PCE, where an error indicator based on the decay rate of local variance was used for an h-adaptive refinement. Its collocation-based counterpart, the multi-element probabilistic collocation method, used the tensor product or sparse grid collocation (Smolyak 1963) in each random element (Foo et al. 2008). A more recent version of the multi-element probabilistic collocation method incorporates the ANOVA (Analysis-of-Variance) decomposition to truncate the PCE at a certain dimension in order to further enhance the computational efficiency (Foo and Karniadakis 2010). In addition to the multi-element PCE, a sparse polynomial chaos approximation was introduced as an alternative to tensor product polynomial bases (Todor and Schwab 2007) and a sparse stochastic collocation method based on this sparse basis was recently developed in Bieri and Schwab (2009). Although these adaptive algorithms alleviate the curse of dimensionality to some degree, more efforts are still needed to fully resolve this difficulty. As demonstrated by Lee and Chen (2007), the implementation of the PCE method becomes inconvenient in engineering design practice since the PCE order cannot be predetermined for black-box-type problems.

This paper thus presents an adaptive-sparse polynomial chaos expansion (adaptive-sparse PCE) method for reliability analysis and design of complex engineering systems. To overcome the curse of dimensionality of the PCE method, this research first proposes an adaptive-sparse expansion scheme. This scheme automatically detects the most significant bivariate terms and adaptively builds the sparse PCE with the minimum number of bivariate basis functions. Moreover, the adaptive-sparse scheme offers the additional capability of automatically adjusting the PCE order to optimize the accuracy of the stochastic response surface. To make the proposed method computationally tractable for engineering design, the projection technique used in the

EDR method is employed to effectively compute the expansion coefficients. Moreover, a copula theory is successfully integrated to the proposed adaptive-sparse PCE method, which enables the designer to handle nonlinear correlation of input random variables.

Section 2 of this paper reviews the generalized PCE method for the effective functional representation of stochastic variability. Section 3 presents the adaptive-sparse PCE method and introduces the error decomposition scheme. The proposed ideas are demonstrated using several case studies in Section 4. Section 5 concludes this paper.

## 2 Review of polynomial chaos expansion (PCE) method

In the following sections, we will model the $N$-dimensional real random variables $\mathbf{x} = (x_1, x_2, ..., x_N)^{\mathrm{T}}$ in a complete probability space $(\Omega, \mathcal{A}, \Pi)$, where $\Omega$ is a sample space, $\mathcal{A}$ is a $\sigma$-algebra on $\Omega$, and $\Pi$ is a probability measure function $\Pi$: $\mathcal{A} \rightarrow [0, 1]$. Then the probability density function (PDF) of the random variable $x_i$ defines a probability mapping $f_i(x_i)$: $\Gamma_i \rightarrow \mathbb{P}^+$, where the support $\Gamma_i$ is a one-dimensional random space of $x_i$. Under the assumption of independence, the probabilistic characteristics of the random variables $\mathbf{x}$ can be completely defined by the joint PDF $f(\mathbf{x}) = f_1(x_1) \cdot f_2(x_2) \cdots f_N(x_N)$ with the support $\Gamma = \Gamma_1 \cdot \Gamma_2 \cdots \Gamma_N$. Let $g(\mathbf{x})$ denote a smooth, measurable performance function on $(\Omega, \mathcal{A})$, which can be treated as a one-to-one mapping between $N$-dimensional space and one-dimensional space $g$: $\mathrm{P}^N \rightarrow \mathbb{P}$. In general, the performance function $g(\mathbf{x})$ cannot be analytically obtained, and the function evaluation of $g$ for a given input $\mathbf{x}$ requires an expensive computer simulation. Therefore, it is important to employ a numerical method for reliability analysis that is capable of producing accurate probabilistic characteristics of $g(\mathbf{x})$ with an acceptably small number of function evaluations.

**Table 1** Type of random inputs and corresponding generalized polynomial chaos basis

| | Random variable | Polynomial chaos | Support |
|---|---|---|---|
| Continuous | Gaussian | Hermite | (−inf, +inf) |
| | Gamma (Exponential) | Generalized Laguerre (Laguerre) | [0,+inf) |
| | Beta | Jacobi | [a,b] |
| | Uniform | Legendre | [a,b] |
| Discrete | Poisson | Charlier | {0,1,...} |
| | Binomial | Krawtchouk | {0,1,...,$N$} |
| | Negative binomial | Meixner | {0,1,...} |
| | Hypergeometric | Hahn | {0,1,...,$N$} |

### 2.1 Generalized PCE method

The original Hermite polynomial chaos, also termed as the homogeneous chaos, was derived from the original theory of Wiener (1938) for the spectral representation of any second-order stochastic response in terms of Gaussian random variables. To improve the expansion convergence rate, Xiu and Karniadakis (2003) extended the method, under the Askey polynomial scheme, to non-Gaussian random variables (e.g., gamma, uniform, and beta). The types of random variables and the corresponding orthogonal polynomial families are listed in Table 1. In the finite dimensional random space $\Gamma$, a second-order stochastic response $g$ can be expanded in a convergent series of generalized polynomial chaos basis as

$$\begin{aligned} g(\mathbf{x}) = c_0\psi_0 &+ \sum_{i_1=1}^{\infty} c_{i_1}\psi_1\left(\zeta_{i_1}(\mathbf{x})\right) \\ &+ \sum_{i_1=1}^{\infty}\sum_{i_2=1}^{i_1} c_{i_1 i_2}\psi_2\left(\zeta_{i_1}(\mathbf{x}), \zeta_{i_2}(\mathbf{x})\right) \\ &+ \sum_{i_1=1}^{\infty}\sum_{i_2=1}^{i_1}\sum_{i_3=1}^{i_2} c_{i_1 i_2 i_3}\psi_3\left(\zeta_{i_1}(\mathbf{x}), \zeta_{i_2}(\mathbf{x}), \zeta_{i_3}(\mathbf{x})\right) + \cdots \end{aligned} \tag{2}$$

where $\psi_n(\zeta_{i_1}(\mathbf{x}), \zeta_{i_2}(\mathbf{x}), ..., \zeta_{i_n}(\mathbf{x}))$ denotes the $n$-dimensional Askey-chaos of order $n$ in terms of the random variables $\{\zeta_{i_1}, \zeta_{i_2}, ..., \zeta_{i_n}\}$. According to the Cameron-Martin theorem (Cameron and Martin 1947), the polynomial chaos expansion in (2) converges in the $L_2$ sense.

For the purpose of notational convenience, (2) is often rewritten as

$$g(\mathbf{x}) = \sum_{i=0}^{\infty} s_i \Phi_i\left(\zeta(\mathbf{x})\right), \qquad \zeta = \{\zeta_1, \zeta_2, \ldots\} \tag{3}$$

where there exists a one-to-one mapping between the polynomial basis functions $\psi_n$ and $\Phi_i$, and the PCE coefficients $s_i$ and $c_{i_1,...,i_r}$.

The orthogonality of the Askey-chaos can be expressed as

$$E\left[\Phi_i \Phi_j\right] = \delta_{ij} E\left[\Phi_i^2\right] \tag{4}$$

where $\delta_{ij}$ is the Kronecker's delta and $E[\cdot]$ is the expectation operator. Considering all $N$-dimensional polynomials of degree not exceeding $p$ gives the truncated PCE as

follows (with $P$ denoting the number of unknown PCE coefficients):

$$g(\mathbf{x}) = \sum_{i=0}^{P-1} s_i \Phi_i(\zeta), \qquad \mathbf{x} = \{x_1, x_2, \ldots, x_N\},$$
$$\zeta = \{\zeta_1, \zeta_2, \ldots \zeta_N\} \tag{5}$$

In the above summation, the number of unknown PCE coefficients $P$ is

$$P = \binom{N+p}{p} = \frac{(N+p)!}{N!p!} \tag{6}$$

### 2.2 Determination of PCE coefficients

In this study, the reliability analysis for the performance function $g$ under random inputs $\mathbf{x}$ is of our interest. Since the uncertainty of a stochastic response $g$ can be fully characterized by the PCE coefficients in (3), an efficient and accurate numerical procedure to compute the coefficients is essential for reliability analysis.

Based on the orthogonality of the polynomial chaos, the projection method (Le Maître et al. 2001, 2002) can be used as a non-intrusive approach to compute the expansion coefficients of a response. Pre-multiplying both sides of (3) by $\Phi_j(\zeta)$ and taking the expectation gives the following equation

$$E\left[g(\mathbf{x})\Phi_j(\zeta)\right] = E\left[\sum_{i=0}^{\infty} s_i \Phi_i(\zeta)\Phi_j(\zeta)\right] \tag{7}$$

Due to the orthogonality of the polynomial chaos, (7) takes the form

$$s_j = \frac{E\left[g(\mathbf{x})\Phi_j(\zeta)\right]}{E\left[\Phi_j^2(\zeta)\right]} \tag{8}$$

In this expression, the denominator can be readily obtained in an analytical form, while the numerator may require a multi-dimensional integration. This integration may be accomplished by the full tensorization of one-dimensional Gaussian quadrature (Le Maître et al. 2002), the crude MCS (Field 2002), or the Smolyak sparse grid (Smolyak 1963; Gerstner and Griebel 1998, 2003; Ma and Zabaras 2009). The relative merits and disadvantages of these approaches are discussed below:

Approach 1 The full tensorization of one-dimensional Gaussian quadrature exhibits fast convergence for smooth integrand. However, the computational cost grows exponentially with the dimension $N$: $M = M_1^N$, which is known as the ''curse of dimensionality''. Here, $M$ denotes the total number of function evaluations and $M_1$ denotes the number of one-dimensional quadrature points. To prevent large integration errors, $M_1$ should be at least equal to the PCE order $p$.

Approach 2 The crude MCS is robust and has a convergence rate that is independent of the dimension $N$ asymptotically (Xiu 2009). However, the convergence is very slow (as $1/\sqrt{M}$). Thus, accurate results require a large number of function evaluations which may incur intolerable computational burden, especially for complex engineered systems that are computationally intensive.

Approach 3 The sparse grid collocation based on the Smolyak algorithm (Smolyak 1963) offers an alternative way for the multidimensional integration (Gerstner and Griebel 1998). Compared with the fully tensorized quadrature, it also achieves fast convergence for smooth integrand but with much lower computational cost. Recently, adaptive algorithms (Gerstner and Griebel 2003; Ma and Zabaras 2009) have been developed that further reduce the computational cost. However, the sparse grid collocation methods still cannot fully resolve the difficulty induced by the ''curse of dimensionality''.

## 3 Adaptive-sparse polynomial chaos expansion (PCE) method

As an attempt to address the challenges described in Section 2.2, an adaptive-sparse polynomial chaos expansion is introduced in this section. The proposed method involves: (i) an adaptive-sparse scheme for the PCE method, (ii) a decomposition-based projection method for efficiently computing the expansion coefficients, (iii) an integration of copula to handle nonlinear correlation of input random variables. An error decomposition scheme is provided as well.

### 3.1 Adaptive-sparse scheme

The aim of this section is to develop an adaptive-sparse scheme for obtaining the minimum number of bivariate terms. Due to the inherent characteristics of orthogonal polynomials, we will use the PCE as the projection basis to make

the adaptive-sparse scheme computationally efficient and convergent. It is expected that the PCE model resulting from the adaptive-sparse scheme will achieve an optimal compromise between the UDR and BDR (more accurate than the UDR and more efficient than the BDR).

This scheme mainly consists of two loops to determine: (outer loop) the number ($q$) of the most significant bivariate terms (denoted as a set $\mathbf{B}$), and (inner loop) the optimal expansion order $p$. The detailed procedures are listed as follows:

Initialization

(a) Initialize $p = 2$, $q = 0$, $\mathbf{B} = \emptyset$, and set the convergence criteria $\varepsilon_1$ and $\varepsilon_2$ for the outer and inner loops, respectively.

(b) Compute the values of the performance function $g(\mathbf{x})$ at the univariate sample points: $g(\boldsymbol{\mu})$, $g\left(x_k^{(i_k)},\ \boldsymbol{\mu}^k\right)$, for $i_k = 1, 2, ..., M_1$, $k = 1, 2, ..., N$, where the superscript $i_k$ denotes the corresponding sample point for $x_k$, $M_1$ the number of univariate sample points in each dimension, and $\boldsymbol{\mu}^k$ the mean vector of input random variables excluding $x_k$.

(c) With the function values obtained in step (b), construct a 2nd order PCE by computing the coefficients of univariate polynomial terms while setting the other coefficients to zero. The method for computing the PCE coefficients will be detailed in the subsequent section.

Outer loop

(d) Compute the values of $g(\mathbf{x})$ at the $N(N-1)/2$ bivariate sample points which correspond to $N(N-1)/2$ pairs of variables: $g\left(x_k^t, x_l^t, \boldsymbol{\mu}^{k,l}\right)$, for $k,l = 1, 2, ..., N$, $k < l$, where $\boldsymbol{\mu}^{k,l}$ denotes the mean vector of input random variables excluding $x_k$ and $x_l$. Based on the function values, compute the error indicators for all $N(N-1)/2$ bivariate terms. Note that, for computing the error indicators, we do not require all the bivariate sample points that are used to compute the coefficients for each bivariate term, but use only one sample point for each bivariate term. An error indicator for testing the bivariate interaction between $k$th and $l$th input variables $[x_k, x_l]$ is defined as

$$e_{kl} = \frac{\left|\hat{g}_{(u)}\left(x_k^t, x_l^t, \boldsymbol{\mu}^{k,l}\right) - g\left(x_k^t, x_l^t, \boldsymbol{\mu}^{k,l}\right)\right|}{\max\limits_{1\le i_j\le M_1, 1\le j\le N}\left\{g\left(x_j^{(i_j)}, \boldsymbol{\mu}^j\right)\right\} - \min\limits_{1\le i_j\le M_1, 1\le j\le N}\left\{g\left(x_j^{(i_j)}, \boldsymbol{\mu}^j\right)\right\}} \tag{9}$$

where $\hat{g}_{(u)}\left(x_k^t, x_l^t, \boldsymbol{\mu}^{k,l}\right)$ is the functional approximation at $\left(x_k^t, x_l^t, \boldsymbol{\mu}^{\kappa,l}\right)$ by a response approximation method using the function values at the univariate sample points. For the response approximation, we use the stepwise moving least squares (SMLS) method of which the details can be found in the author's previous work (Youn et al. 2007a). In this study, we apply $x_k^t = \mu_k + 3\sigma_k$ and $x_l^t = \mu_l + 3\sigma_l$, where $\mu_k$ and $\mu_l$ denote the means, and $\sigma_k$ and $\sigma_l$ denote the standard deviations of $x_k$ and $x_l$. The numerator in (9) can be treated as the absolute univariate approximation error induced by the bivariate interaction, while the denominator can be treated as a normalization factor. Since the error indicator provides the relative ranking of bivariate interactions rather than the absolute estimates, it may not be necessary to employ multiple test sample points for each bivariate term. A larger error indicator implies a stronger interaction between a given pair of variables. The pairs of variables with stronger interaction are given a higher priority in the algorithm since the inclusion of the pairs is likely to reduce a numerical error more significantly in probability analysis.

(e) Add the bivariate term $\left[x_k^{q+1},\ x_l^{q+1}\right]$ with the $(q+1)$th largest error indicator to the bivariate set: $\mathbf{B} = \mathbf{B} \cup \left\{\left[x_k^{q+1},\ x_l^{q+1}\right]\right\}$ and increase the number of bivariate terms: $q = q + 1$. Compute the function values of $g(\mathbf{x})$ at the bivariate sample points corresponding to the bivariate term $\left[x_k^{q+1},\ x_l^{q+1}\right]$.

(f) With the function values obtained in step (e), compute the coefficients of bivariate polynomial terms in the constructed PCE model. The method for computing the PCE coefficients will be detailed in the subsequent section.

Inner Loop

(g.1) If $q = 1$, we intend to determine the optimum PCE order through a convergence analysis. For this purpose, we need an error estimate to assess the performance of the constructed $p$th order PCE (or stochastic response surface) $\hat{g}_p$. We prefer an efficient error estimate of which the evaluation only requires the already obtained response values at the sample points $\mathbf{x}^{(i)}$, for $1 \le i \le M$, where $M$ is the total number of sample points. In this study, we use the coefficient of determination $R^2$, which can be

defined based on the residual sum of squares $e_{RSS}$ and total sum of squares $e_{TSS}$ as

$$R^2(\hat{g}_p) = 1 - \frac{e_{RSS}(\hat{g}_p)}{e_{TSS}} \tag{10}$$

where

$$e_{RSS}(\hat{g}_p) = \frac{1}{M}\sum_{i=1}^{M}\left(g(\mathbf{x}^{(i)}) - \hat{g}_p(\mathbf{x}^{(i)})\right)^2 \tag{11}$$

and

$$e_{TSS} = \frac{1}{M}\sum_{i=1}^{M}\left(g(\mathbf{x}^{(i)}) - \bar{g}\right)^2; \quad \bar{g} = \frac{1}{M}\sum_{i=1}^{M} g(\mathbf{x}^{(i)}) \tag{12}$$

We note that the cross-validation based errors (Kohavi 1995), which have been widely used in the machine learning technique to evaluate the model performance, can also be used as error estimates and deserve future studies.

(g.2) Increase the PCE order: $p = p + 1$.

(g.3) Repeat the steps (g.1) and (g.2) until $R^2$ converges to within a relative tolerance of $\varepsilon_2$.

Postprocessor

(h) Compute the reliability value based on the constructed PCE model. The numerical method for estimating the reliability will be detailed in the subsequent section.

(i) Repeat the steps from (e) to (h) until the value of reliability converges to within a relative tolerance of $\varepsilon_1$.

The completion of the adaptive-sparse algorithm entails the optimal determination of the set **B** of bivariate terms and the PCE order $p$. The resultant PCE model should guarantee the most accurate and cost-effective fit among all bivariate PCE models.

## 3.2 Decomposition-based projection method

This section presents a decomposition-based projection method for efficiently computing the expansion coefficients of an optimum set of uni- and bivariate polynomial terms. The proposed method attempts to further reduce the computational cost of the projection method.

### 3.2.1 *Uni- and bivariate dimension reduction*

Let $\boldsymbol{\mu}^i$ = denote the mean vector of input random variables excluding $x_i$, and let $\boldsymbol{\mu}^{i_1,i_2}$ denote the mean vector of input random variables excluding $x_{i_1}$ and $x_{i_2}$. Depending on the levels of the decomposition, the uni- and bivariate decomposed responses (Xu and Rahman 2004) can be expressed as, respectively,

$$g_1(\mathbf{x}) = \sum_{i=1}^{N} g(x_i, \boldsymbol{\mu}^i) - (N-1)g(\boldsymbol{\mu}) \tag{13}$$

and

$$g_2(\mathbf{x}) = \sum_{1\le i_1<i_2\le N} g(x_{i_1}, x_{i_2}, \boldsymbol{\mu}^{i_1,i_2}) - (N-2)\sum_{i=1}^{N} g(x_i, \boldsymbol{\mu}^i) + \frac{(N-1)(N-2)}{2} g(\boldsymbol{\mu}) \tag{14}$$

It is important to note that the univariate decomposed response $g_1$ in (13) contains the univariate terms $g(x_i, \boldsymbol{\mu}^i)$ of any order in the Taylor series expansion and, similarly, the bivariate decomposed response $g_2$ in (14) has all bivariate terms in the Taylor series expansion. Thus, the approximations in (13) and (14) should not be viewed as first- or second-order Taylor series expansion nor do they represent a limited degree of nonlinearity in $g(\mathbf{x})$. In fact, the residual error of a univariate approximation to a multidimensional integration of a system response over a symmetric domain contains only even-order terms of dimensions two and higher since the integrations of odd-order terms become zeros for a symmetric integration domain. This residual error was reported to be far less than that of a second-order Taylor expansion method for probability analysis (Rahman and Xu 2004).

### 3.2.2 *Formulation of decomposition-based projection method*

To compute the coefficient of any $n$th-order univariate polynomial term $\Psi_n(\zeta_k(\mathbf{x}),..., \zeta_k(\mathbf{x}))$ in (2), which corresponds to a univariate polynomial term $\Phi_j(\zeta_k)$ in (3), the proposed decomposition-based projection method uses the univariate decomposed response in (13) (Xu and Rahman 2004). The

expansion coefficients can be obtained by projecting the univariate terms onto $g(\mathbf{x})$ as

$$s_j^k = \frac{E\left[g(\mathbf{x})\Phi_j(\zeta_k)\right]}{E\left[\Phi_j^2(\zeta_k)\right]} \cong \frac{\sum_{i=1}^{N} E\left[g\left(x_i, \boldsymbol{\mu}^i\right)\Phi_j(\zeta_k)\right] - (N-1)\, g(\boldsymbol{\mu}) E\left[\Phi_j(\zeta_k)\right]}{E\left[\Phi_j^2(\zeta_k)\right]} = \frac{E\left[g\left(x_k, \boldsymbol{\mu}^k\right)\Phi_j(\zeta_k)\right]}{E\left[\Phi_j^2(\zeta_k)\right]} \tag{15}$$

Similarly, the coefficient of any $n$th-order bivariate polynomial term $\Psi_n(\zeta_k(\mathbf{x}), ..., \zeta_l(\mathbf{x}))$ in (2), which corresponds to a bivariate polynomial term $\Phi_j(\zeta_k, \zeta_l)$ in (3), can be computed using the decomposition-based projection method. This method makes use of the bivariate decomposed response in (14) (Xu and Rahman 2004). The expansion coefficients can be obtained by projecting the bivariate terms onto $g(\mathbf{x})$ as

$$s_j^{k,l} = \frac{E\left[g(\mathbf{x})\Phi_j(\zeta_k, \zeta_l)\right]}{E\left[\Phi_j^2(\zeta_k, \zeta_l)\right]} \cong \frac{\left\{\begin{array}{l} \sum_{1\le i_1<i_2\le N} E\left[g\left(x_{i_1}, x_{i_2}, \boldsymbol{\mu}^{i_1,i_2}\right)\Phi_j(\zeta_k, \zeta_l)\right] \\ \quad - (N-2)\sum_{i=1}^{N} E\left[g_i\left(x_i, \boldsymbol{\mu}^i\right)\Phi_j(\zeta_k, \zeta_l)\right] \\ \quad + \frac{(N-1)(N-2)}{2} E\left[g(\boldsymbol{\mu})\Phi_j(\zeta_k, \zeta_l)\right] \end{array}\right\}}{E\left[\Phi_j^2(\zeta_k, \zeta_l)\right]} = \frac{E\left[g\left(x_k, x_l, \boldsymbol{\mu}^{k,l}\right)\Phi_j(\zeta_k, \zeta_l)\right]}{E\left[\Phi_j^2(\zeta_k, \zeta_l)\right]} \tag{16}$$

It is noted that (15) and (16) requires only one- and two-dimensional integrations and are computationally more efficient than performing the $N$-dimensional integration in (8). Thus, the computational cost in calculating the coefficient of any uni- or bivariate polynomial term is substantially reduced by using the decomposition-based projection method. Similarly, the decomposition-based projection can be extended to compute the coefficients of tri- and higher-variate polynomial terms. However, the coefficient of any tri- or higher-variate polynomial term is treated as zero in this study. This is because of the following two facts: (i) for most engineering problems, considering the interaction between two variables (i.e., the bivariate interaction) is sufficient to yield very accurate statistical results (Xu and Rahman 2004), and (ii) the calculations of tri- and higher-variate polynomial coefficients require a substantially larger amount of computational effort, which may make the method computationally intolerable.

#### 3.2.3 *Numerical procedure of decomposition-based projection method*

The numerical integration is required to evaluate the one- and two-dimensional integrations in (15) and (16). The most straightforward and efficient way is to directly use the Gaussian quadrature, where Gauss-Hermite, Gauss-Legendre, and Gauss-Jacobi quadrature rules determine the integration points and associated weights for a random variable following Gaussian, Uniform, and Beta distributions, respectively. However, a low-order Gaussian quadrature rule often leads to large errors in computing the coefficients of high-order PCE terms. To enhance the stability and accuracy of the Gaussian quadrature, we first use the stepwise moving least squares (SMLS) method (Youn et al. 2007a; Youn and Choi 2004b) to construct uni- and bivariate response approximations with the response values evaluated at the predefined samples points, and then carry out the Gaussian quadrature integrations with a large number of integration points (or a high-order quadrature rule) from the approximate responses. Note that the uni- and bivariate sample points used to construct the response approximations should not be confused with the integration points in the Gaussian quadrature. Thus, even if the PCE order $p$ is increased, the numbers of uni- and bivariate sample points may not necessarily be increased as long as the response approximations by the SMLS are sufficiently accurate. More detailed information regarding the SMLS and Gaussian quadrature for integrations can be found in the author's previous work (Youn et al. 2007a).

### 3.3 Copula for nonlinear correlation modeling

In many structural reliability analysis and design problems, it is highly probable that the input random variables such as material properties and fatigue properties are correlated (Noh et al. 2008). In this case, the reliability analysis and design require a joint CDF for the exact transformation of the correlated random variables into uncorrelated standard normal random variables. However, it requires an infinite amount of data to acquire the true joint CDF. In contrast, a copula only requires marginal CDFs and a dependence structure to formulate an approximate joint CDF. Thus, the selection of dependence structure and formulation of the joint CDF can be done with a limited amount of data (Noh et al. 2008).

### 3.3.1 Introduction of copula

In statistics, a copula is defined by Roser (1999) as ''a function that joins or couples multivariate joint distribution functions to their one-dimensional marginal distribution functions'', or ''multivariate distribution functions whose one-dimensional margins are uniform on the interval [0,1]''.

Let $F$ be an $N$-dimensional cumulative distribution function (CDF) with continuous marginal CDFs $F_1$, $F_2$, ..., $F_N$. Then according to Sklar's theorem, there exists a unique $N$-copula $C$ such that

$$F(x_1, x_2, ..., x_N) = C(F_1(x_1), F_2(x_2), ..., F_N(x_N)) \quad (17)$$

It then becomes clear that a copula formulates a joint CDF with the support of separate marginal CDFs and a dependence structure. The copula is capable of constructing the joint CDF in real applications with different types of marginal CDFs or dependence structures. Various general types of dependence structures can be represented, corresponding to various copula families, such as Gaussian, Clayton, Frank, and Gumbel. Let $u_i = F_i(x_i)$, i = 1, 2,..., $N$, a $N$-dimensional Archimedean copula is defined as

$$C(u_1, u_2, \cdots, u_N|\alpha) = \Psi_\alpha^{-1}\left(\sum_{i=1}^{N} \Psi_\alpha(u_i)\right) \quad (18)$$

where $\Psi_\alpha$ denotes a generator function with a correlation parameter $\alpha$ and satisfies the following conditions:

$$\Psi_\alpha(1) = 0; \quad \lim_{u\to 0} \Psi_\alpha(u) = \infty;$$
$$\frac{d}{du}\Psi_\alpha(u) < 0; \quad \frac{d^2}{du^2}\Psi_\alpha(u) > 0 \quad (19)$$

Let $\Psi_\alpha(u) = u^\alpha - 1$ and $N = 2$, then we formulate a bivariate Clayton copula as

$$C(u_1, u_2|\alpha) = \left(u_1^{-\alpha} + u_2^{-\alpha} - 1\right)^{-1/\alpha} \quad (20)$$

More detailed information on copula families can be found in Roser (1999) and Noh et al. (2008).

### 3.3.2 Rosenblatt transformation

The Rosenblatt transformation has been used extensively for mapping the correlated random variables onto the independent standard normal variables (Rosenblatt 1952). The successive conditioning procedures for a vector of correlated random variables are defined as

$$\begin{aligned} z_1 &= \varphi^{-1}\left[F_1(x_1)\right] \\ z_2 &= \varphi^{-1}\left[F_2(x_2|x_1)\right] \\ &\vdots \\ z_N &= \varphi^{-1}\left[F_N(x_N|x_1, x_2, \cdots, x_{N-1})\right] \end{aligned} \quad (21)$$

where $z_1, z_2, ..., z_N$ denote the independent standard random variables after the transformation, $\phi^{-1}(\cdot)$ denotes the inverse CDF of a standard normal variable, $F_i(x_i|x_1, x_2, ..., x_{i-1})$ denotes the CDF of $x_i$ conditioned on $X_1 = x_1$, $X_2 = x_2$, ..., $X_{i-1} = x_{i-1}$, and can be expressed as

$$F_i(x_i|x_1, x_2, \cdots, x_{i-1}) = \frac{\int_{-\infty}^{x_i} f_i(x_1, x_2, \cdots, x_{i-1}, \tau)d\tau}{f_{i-1}(x_1, x_2, \cdots, x_{i-1})} \quad (22)$$

where $f_i(x_1, x_2, ..., x_i)$ denotes the marginal joint PDF of $x_1, x_2, ..., x_i$.

To use the Rosenblatt transformation for the purpose of reliability analysis and design, the joint CDF of input random variables should be available. However, it is very difficult to obtain the joint CDF in real applications. In contrast, a copula can easily formulate an approximate joint CDF based on separate marginal CDFs and correlation parameters, which can be practically obtained from limited experimental data (Noh et al. 2008). The Rosenblatt transformation for a bivariate copula is given as

$$\begin{aligned} z_1 &= \varphi^{-1}[u_1] = \varphi^{-1}\left[F_1(x_1)\right] \\ z_2 &= \varphi^{-1}\left[C(u_2|u_1)\right] = \varphi^{-1}\left[C\left(F_2(x_2)|F_1(x_1)\right)\right] \end{aligned} \quad (23)$$

where

$$\begin{aligned} C(u_2|u_1) &= P(U_2 \le u_2|U_1 = u_1) \\ &= \lim_{\Delta u_1 \to 0} \frac{C(u_1 + \Delta u_1, u_2) - C(u_1, u_2)}{\Delta u_1} \\ &= \frac{\partial C(u_1, u_2)}{\partial u_1} \end{aligned} \quad (24)$$

After the Rosenblatt transformation, the independent standard random variables are used as the Gaussian input variables for the generalized PCE with Hermite polynomial basis. A vehicle side-crash example in Section 5 will illustrate the feasibility of the proposed method.

## 3.4 Reliability and sensitivity analysis

### 3.4.1 Reliability analysis

Once the uni- and bivariate PCE coefficients are calculated, an approximate function of the original implicit performance function $g$ is obtained as

$$\begin{aligned} \hat{g}(\mathbf{x}) = g(\boldsymbol{\mu}) &+ \sum_{k=1}^{N} \sum_{j} s_j^k \Phi_j\left(\zeta_k(x)\right) \\ &+ \sum_{k,l=1;k<l}^{N} \sum_{j} s_j^{k,l} \Phi_j\left(\zeta_k(\mathbf{x}), \zeta_l(\mathbf{x})\right) \end{aligned} \quad (25)$$

The above expression can be viewed as an explicit mapping $\hat{g}$: $\mathrm{P}^N \rightarrow \mathbb{P}$, which approximates the exact implicit mapping $g$: $\mathrm{P}^N \rightarrow \mathbb{P}$. Thus, any probabilistic characteristics of $g(\mathbf{x})$, including statistical moments, reliability, and PDF, can be easily estimated by performing MCS. For example, any $r$th moment can be calculated as

$$m_r \cong \int \hat{g}^r(\mathbf{x}) f(\mathbf{x}) d\mathbf{x} = E\left(\hat{g}^r(\mathbf{x})\right) = \lim_{ns\to\infty} \frac{1}{ns} \sum_{k=1}^{ns} \hat{g}^r\left(\mathbf{x}^{(k)}\right) \tag{26}$$

where $m_r$ is the $r$th moment of the performance function $g$; $f(\mathbf{x})$ is the joint PDF; $\mathbf{x}^{(k)}$ is the $k$th realization of $\mathbf{x}$; and $ns$ is the sampling size. It is noted that, although MCS is used to compute the moments due to its convenience, it is not required since moments of a PCE can be analytically obtained. Low-order moments (e.g., mean and variance) have simple analytical forms while high-order moments, for which orthogonality cannot be fully exploited, possess complicated forms. For reliability calculation, let us define an approximate safe domain for the performance function $g$ as

$$\hat{\Omega}^S = \left\{\mathbf{x} : \hat{g}(\mathbf{x}) < 0\right\} \tag{27}$$

Therefore, the reliability $R$ can also be estimated by performing MCS as

$$R \cong \int I_{\hat{\Omega}^S}(\mathbf{x}) f(\mathbf{x}) d\mathbf{x} = E\left(I_{\hat{\Omega}^S}(\mathbf{x})\right) = \lim_{ns\to\infty} \frac{1}{ns} \sum_{k=1}^{ns} I_{\hat{\Omega}^S}\left(\mathbf{x}^{(k)}\right) \tag{28}$$

where $I[\cdot]$ is an indicator function of safe or fail state such that

$$I_{\hat{\Omega}^S}\left(\mathbf{x}^{(k)}\right) = \begin{cases} 1, & \mathbf{x}^{(k)} \in \hat{\Omega}^S \\ 0, & x^{(k)} \in \Omega \backslash \hat{\Omega}^S \end{cases} \tag{29}$$

It should be noted that the MCS performed here is inexpensive because it employs the explicit representation function in (25).

#### *3.4.2 Probabilistic sensitivity analysis*

In reliability-based design optimization (RBDO), probabilistic sensitivity analysis is required to identify the effect of the change in the parameters of random variables upon the change in reliability or moments. Since MCS is used for evaluating the statistical properties (e.g., $r$th moment, reliability) of a response in the adaptive-sparse PCE method, this study computes the probabilistic sensitivity of the response with respect to a random variable using a finite difference method (FDM). The FDM uses the original and perturbed values of moments or reliabilities to computes their sensitivities.

The sensitivity of any $r$th moment and reliability with respect to the $j$th element $\theta_j$ (e.g., $\mu$, or $\sigma$, etc.) in a vector of deterministic distribution parameters $\boldsymbol{\theta}$ is computed using (30) and (31), respectively.

$$\frac{\partial m_r(\boldsymbol{\theta})}{\partial \theta_j} \cong \frac{m_r(\theta_j + \Delta\theta_j) - m_r(\theta_j)}{\Delta\theta_j} \tag{30}$$

$$\frac{\partial R(\boldsymbol{\theta})}{\partial \theta_j} \cong \frac{R(\theta_j + \Delta\theta_j) - R(\theta_j)}{\Delta\theta_j} \tag{31}$$

where $m_r(\boldsymbol{\theta})$ is the $r$th moment of the constraint $G$ (or the cost function $C$); $\Delta\theta_j$ is the perturbed value of $\theta_j$. A perturbation size of 0.1% is employed in this study. It is noted that, for computing a perturbed moment or reliability, an extra MCS based on the approximate response model in (25) is used without extra computational cost. For the extra MCS, the random number seeds for the original MCS should be reused to reduce numerical noise and obtain a stable sensitivity estimate. As an alternative to the FDM, the score function can also be used to compute the probabilistic sensitivities (Rahman 2009) and we observed similar performance. An accuracy study will be conducted in Section 5 to demonstrate the effectiveness of the proposed method for probabilistic sensitivity analysis.

### 3.5 Computational procedure

The overall computation procedure is shown in Fig. 1. If nonlinear correlation exists between the random inputs $\mathbf{x}$, the copula is employed to model the joint PDF $f(\mathbf{x})$ and the Rosenblatt transformation to transform $\mathbf{x}$ to independent standard normal variables $\mathbf{z}$. The computations of PCE coefficients $s_j^k$ in (15) require the response values (i.e., values of the performance function) at the univariate sample points: $g(\boldsymbol{\mu})$, $g\left(x_k^{(i_k)}, \boldsymbol{\mu}^k\right)$, for $i_k = 1, 2, ..., M_1$, where the superscript $i_k$ denotes the corresponding sample point for $x_k$ and $M_1$ the number of univariate sample points in each dimension. The computations of PCE coefficients $s_j^{k,l}$ in (16) require the response values at the bivariate sample points: $g\left(x_k^{(i_{k,l})}, x_l^{(i_{k,l})}, \boldsymbol{\mu}^{k,l}\right)$, for $i_{k,l} = 1, 2, ..., M_2$, where the superscript $i_{k,l}$ denotes the corresponding bivariate sample points for the bivariate term $[x_k, x_l]$, and $M_2$ the number of bivariate sample points for each bivariate term. Thus, the total number of function evaluations for the adaptive-sparse PCE with $q$ bivariate terms is $q(M_2 - 1) + N(N -$

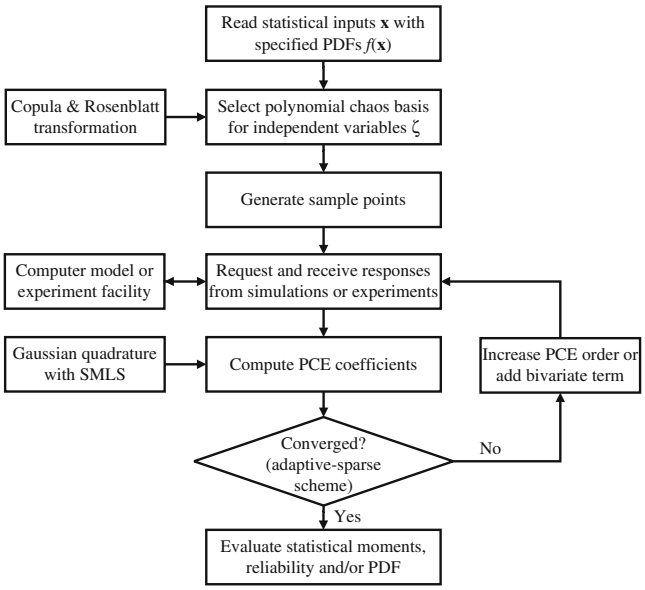


**Fig. 1** Flowchart of the adaptive-sparse algorithm

$1)/2+(M_1-1)N+1$. Below are several important remarks regarding the properties of the adaptive-sparse PCE.

*Remark 1* The $N$-variate, $p$th-order adaptive-sparse PCE is a finite sum of uni- and bivariate polynomial terms up to the $p$th order, with the coefficient of any tri- or higher-variate polynomial term being zero. Thus, if the tri- and higher-variate interactions are negligible, the adaptive-sparse PCE gives an accurate approximation of the function $g$, with a lower computational effort than the conventional PCE. Otherwise, numerical error in the adaptive-sparse PCE may be stacked up due to the tri- and higher-variate interactions. More detailed error analysis will be given in the subsequent section.

*Remark 2* The uni- and bivaraite dimension reduction methods have been extensively studied for reliability analysis and design by previous researchers (Rahman and Xu 2004; Xu and Rahman 2004; Youn et al. 2007a; Rahman 2006, 2009; Lee et al. 2008). However, no attempt has been made to optimize the number of the bivariate terms to be considered for probability analysis. The common approach either depends on the univariate dimension reduction (UDR) (Rahman and Xu 2004; Youn et al. 2007a; Lee et al. 2008) or makes comparison with its bivairate counterpart, bivariate dimension reduction (BDR) (Xu and Rahman 2004; Rahman 2006, 2009). The method developed here uses the error indicator in (9) to adaptively add the bivariate terms to the PCE model until a convergence criterion is achieved. This adaptive process takes advantage of the PCE as the projection basis. The inherent characteristics of orthogonal polynomials make the adaptive process computationally efficient and convergent. Therefore, we argue that the adaptive-sparse PCE achieves an optimal compromise between the UDR and BDR (more accurate than the UDR and more efficient than the BDR).

*Remark 3* In addition to the Rosenblatt transformation, alternative transformation techniques (Noh et al. 2009), such as Nataf transformation, are also capable of transforming Gaussian variables with nonlinear correlation to independent Gaussian variables. In the current study, the non-Gaussian variables with nonlinear correlation are all transformed to independent Gaussian variables. However, it may also be possible to transform the original random variables to independent non-Gaussian variables (e.g., gamma, beta) with distribution types supported by the PCE. Thus, the selections of an appropriate transformation technique and associated procedure are worthy of future studies.

*Remark 4* Through extensive testing with many mathematical and engineering examples, we observed that the parameter setting $\varepsilon_1 = 0.01$ and $\varepsilon_2 = 0.001$ achieves a near-optimum compromise between the accuracy and efficiency. Thus we intended to make this setting as a guideline for implementing the algorithm in most engineering cases. More conservative criteria may give higher accuracy but require more computational effort. Thus, for a specific problem, the optimum $\varepsilon_1$ and $\varepsilon_2$ may vary depending on the requirements on the accuracy and efficiency.

### 3.6 Error decomposition scheme

The proposed adaptive-sparse PCE method integrates the adaptive-sparse scheme and the decomposition-based projection method with the PCE method. It is obvious that

the approximation and numerical schemes produce associated errors in the proposed adaptive-sparse PCE method. This study will therefore analyze the approximation and numerical errors in the proposed method, which provides insights into analyzing the accuracy behavior of the proposed method and properly identifying its potential applications. There are three primary error sources: (i) a PCE truncation error ($\varepsilon_P$), (ii) an error due to a univariate decomposition ($\varepsilon_U$), (iii) an error due to a bivariate decomposition ($\varepsilon_B$), and (iv) an aliasing error ($\varepsilon_I$) which comes from the aliasing error in computing the one- and two-dimensional integrations in (15) and (16) due to the use of two approximation schemes: the SMLS and Gaussian quadrature integration. The total error is a mean-squares error of the $N$-variate, $p$th-order adaptive-sparse PCE with the set $\mathbf{B}$ of bivariate terms and can be decomposed as

$$\begin{aligned}\varepsilon^2 &= \int_\Gamma \left[g(\mathbf{x}) - w^p\left(\zeta(\mathbf{x})\right)\right]^2 f(\mathbf{x})d\mathbf{x} \\ &\le \int_\Gamma \left[g - w^p_{UB}\right]^2 f(\mathbf{x})d\mathbf{x} + \int_\Gamma \left[w^p_{UB} - w^p_U\right]^2 f(\mathbf{x})d\mathbf{x} \\ &\quad + \int_\Gamma \left[w^p_U - w^p_I\right]^2 f(\mathbf{x})d\mathbf{x} + \int_\Gamma \left[w^p_I - w^p\right]^2 f(\mathbf{x})d\mathbf{x} \\ &= \varepsilon^2_P + \varepsilon^2_B + \varepsilon^2_U + \varepsilon^2_I \end{aligned} \tag{32}$$

The detailed derivation of the four error terms in (32) can be found in the Appendix. A numerical investigation of the first three error terms is provided in Section 4.1.

## 4 Case studies

Seven mathematical and engineering examples are given in this section to demonstrate the effectiveness of the adaptive-sparse PCE method. The first example is a simple mathematical function, which was designed to verify the proposed error decomposition scheme. The subsequent five examples were used for studying the computational accuracy and efficiency of the proposed method for uncertainty quantification and reliability analysis. For comparison purpose, we also employ FORM as a classic reliability analysis method, and the univariate DR (UDR) method (with the Pearson PDF generation system) as a representative of the recently developed moment-based reliability methods (Rahman and Xu 2004; Xu and Rahman 2004; Youn et al. 2007a; Zhao and Ono 2001; Lee and Kwak 2005). In the last example, we carried out reliability-based robust design optimization (RBRDO) for a lower control arm in a high mobility, multipurpose, wheeled vehicle (HMMWV). This case study demonstrates the feasibility of the proposed method in complex product or process design.

### 4.1 Mathematical example: verification of error decomposition scheme

Consider a mathematical function,

$$g(\mathbf{x}) = \sum_{k=1}^{N=5} (x_k - 1)^2 - \sum_{k=3}^{N=5} x^r_k x^r_{k-1} x^r_{k-2} \tag{33}$$

where the five random variables are assumed to be statistically independent and uniformly distributed between 0 and 2. As shown in Section 3.6, the error of the adaptive-sparse PCE method can be decomposed into four parts: $\varepsilon_P$ is the truncation error; $\varepsilon_U$ and $\varepsilon_B$ are the errors induced by the uni- and bivariate decomposed responses in (15) and (16), respectively; $\varepsilon_I$ is the aliasing error. This study investigated the first three error terms. Since the trivariate terms may produce the largest error in the proposed adaptive-sparse PCE method, this example was thus designed to demonstrate an error trend while varying the order ($r$) of the trivariate terms. We evaluated the exact expansion coefficients using a tensor product Gauss-Legendre quadrature technique (Le Maître et al. 2002). For comparison purposes, a relative $L_2$ error norm is defined as Han and Kamber (2000)

$$\eta^2 = \frac{\int_\Gamma \left[g(\mathbf{x}) - \hat{g}(\mathbf{x})\right]^2 f(\mathbf{x})d\mathbf{x}}{\int_\Gamma g(\mathbf{x})^2 f(\mathbf{x})d\mathbf{x}} = \frac{\varepsilon^2}{\mu_g^2 + \sigma_g^2} \tag{34}$$

where $\eta^2$ is the $L_2$ error norm; $\mu_g$ is the mean value of a response $g$; and $\sigma_g$ is the standard deviation of $g$. This relative $L_2$ error norm was used to normalize the three mean-square error terms $\left(\varepsilon^2_P,\ \varepsilon^2_U,\ \text{and}\ \varepsilon^2_B\right)$ in (32). To minimize the aliasing error, we employed the true response and very high order Gaussian quadrature to compute the expectations in (15) and (16). Figure 2 shows the error decomposition results with the PCE order $p = 5$. The three error norms

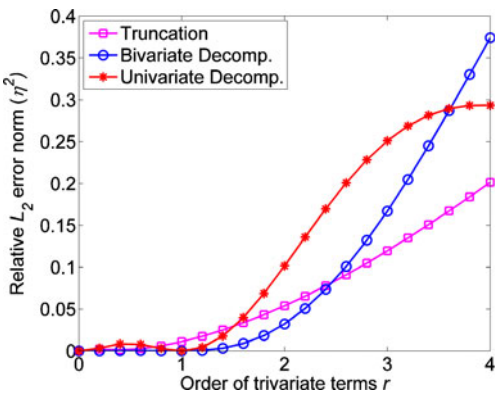


**Fig. 2** Error decomposition results with the increase of the order of trivariate terms

show wide variations from around 0 to 0.4. This indicates that the error of the proposed method strongly depends on the order ($r$) of the trivariate terms. In cases where $r$ is relatively small (<1.4), the truncation error $\eta_P^2$ and univariate decomposition error $\eta_U^2$ dominate, while the error $\eta_B^2$ induced by the bivariate decomposition is negligible because the tri- and higher-variate interactions affecting the response $g$ are very weak. As $r$ increases, the truncation error $\eta_P^2$ becomes no longer dominant, while the error $\eta_B^2$ increases more rapidly than the others, and finally becomes the most significant.

### 4.2 Franke's bivariate test function: unimodal PDF with an irregular shape

This example is found in Franke (1979) and is extensively used for testing a response surface approximation. The Franke bivariate test function is of the form:

$$
\begin{aligned}
g(\mathbf{x}) = & \frac{3}{4}\exp\left(-\frac{(9x_1-2)^2}{4}-\frac{(9x_2-2)^2}{4}\right) \\
& + \frac{3}{4}\exp\left(-\frac{(9x_1+1)^2}{49}-\frac{(9x_2+1)}{10}\right) \\
& + \frac{1}{2}\exp\left(-\frac{(9x_1-7)^2}{4}-\frac{(9x_2-3)^2}{4}\right) \\
& - \frac{1}{4}\exp\left(-(9x_1-4)^2-(9x_2-7)^2\right) \qquad (35)
\end{aligned}
$$

where the random variables are statistically independent and normally distributed with the mean $\mu_1 = \mu_2 = 0.4$, each of which has a 20% coefficient of variation. The response surface has a bimodal characteristic, as shown in Fig. 3a. Using the parameter settings $M_1 = 4$ and $M_2 = 8$, the adaptive-sparse expansion scheme determines the optimal PCE order ($p = 9$). Table 2 presents the adaptive-sparse process of the adaptive-sparse PCE method. Here, a relative error is defined as the absolute error of the estimated reliability divided by the true reliability from MCS. No adaptive procedure for selecting the bivariate terms is required since there is only one bivariate term. The adaptive-sparse PCE method used only 17 simulations to capture the response bimodality and high nonlinearity in the PDF. Figure 3b shows the true PDF by MCS and approximate PDFs by the adaptive-sparse PCE and UDR. Compared to MCS, the adaptive-sparse PCE method shows good accuracy and efficiency, while the UDR is not capable of representing the irregular shape of this PDF. The large error produced by the UDR is mainly due to the following two reasons: (i) errors in moment estimations propagate to errors in PDF construction; and (ii) the first four moments are not sufficient to accurately construct the PDF. To observe the overall PDF and tail-end prediction for reliability analysis, both the moments and probabilities are summarized in Table 3. The limit-state function is defined as $(g - c)$ where a limit-state value $c$ is set to provide different reliability levels. The adaptive-sparse PCE method proved to be more accurate than the other methods for this highly nonlinear problem. Neither FORM nor SORM could provide accurate reliability prediction because of the high nonlinearity.

In addition, the adaptive-sparse PCE method is advantageous because it computes probabilistic sensitivity analysis accurately with no extra cost. Table 3 presents the sensitivities $\partial R_i/\partial \mu_1$ and $\partial R_i/\partial \mu_2$ for $i = 1, 2, 3$ by the adaptive-sparse PCE method and MCS with the finite difference (FD) method. The result of the proposed method is in good agreement with that of MCS.

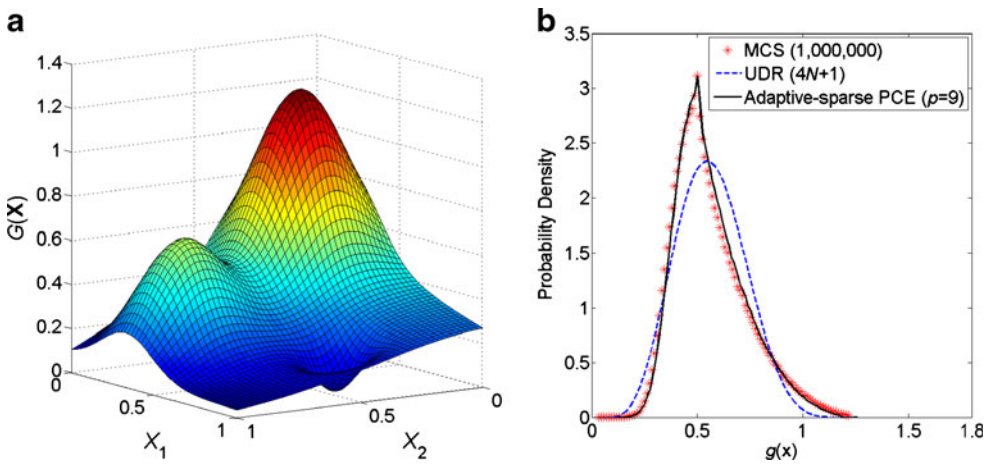


**Fig. 3** Response surface (**a**) and PDF approximations (**b**) for Franke's function

**Table 2** Adaptive-sparse process of the adaptive-sparse PCE for Franke's function ($R_1$)

| | PCE order ($p$) | No. of bivariate terms ($q$) | No. FE | $R^2$ | Reliability | Relative error (%) |
|---|---|---|---|---|---|---|
| Step 1 | 2 | 0 | 9 | 0.73642 | 0.9298 | 3.9463 |
| Step 2 | 2 | 1 | 17 | 0.71477 | 0.9154 | 2.3365 |
| Step 3 | 3 | 1 | 17 | 0.82359 | 0.9079 | 1.4980 |
| Step 4 | 4 | 1 | 17 | 0.96271 | 0.9018 | 0.8161 |
| Step 5 | 5 | 1 | 17 | 0.96482 | 0.9022 | 0.8608 |
| Step 6 | 6 | 1 | 17 | 0.99266 | 0.9011 | 0.7378 |
| Step 7 | 7 | 1 | 17 | 0.99701 | 0.9010 | 0.7267 |
| Step 8 | 8 | 1 | 17 | 0.99179 | 0.9012 | 0.7490 |
| Step 9 | 9 | 1 | 17 | 0.99094 | 0.9013 | 0.7602 |

### 4.3 Fortini's clutch: very low and high reliability levels

This example is the Fortini's clutch shown in Fig. 4. This problem has been extensively used in the field of tolerance design (Creveling 1997; Wu et al. 1998). As shown in Fig. 4, the overrunning clutch is assembled by inserting a hub and four rollers into the cage. The contact angle, $y$, between the vertical line and the line connecting the centers of two rollers and the hub, is expressed in terms of the independent component variables, $x_1$, $x_2$, $x_3$, and $x_4$ as follows:

$$y(\mathbf{x}) = \arccos\left(\frac{x_1 + 0.5(x_2 + x_3)}{x_4 - 0.5(x_2 + x_3)}\right) \tag{36}$$

The statistical information of the random variables is summarized in Table 4. The limit-state function was defined as $(y - c)$ where $c$ specifies a limit-state value. In the adaptive-sparse PCE method, the numbers of univariate and bivariate sample points are selected as follows: $M_1 = 2$ and $M_2 = 8$. For a faster convergence, Jacobi and Hermite polynomial bases were used for $x_1$ and $x_4$, respectively. The error indicators are computed using (9) as follows: $e_{12} = 0.0127$, $e_{13} = 0.0127$, $e_{14} = 0.1183$, $e_{23} = 0.0186$, $e_{24} = 0.0157$, $e_{34} = 0.0157$. Using this information, Table 5 shows the results of the proposed method along the adaptive-sparse procedure where $c = 5°$. The adaptive-sparse scheme was converged with $p = 4$ and $q = 3$. Figure 5 illustrates the PDF evolution along the adaptive-sparse scheme. The PDF approximation was evidently improved from Step 1 to Step 4 by including the most significant bivariate term $[x_1, x_4]$ into the PCE model. On the other hand, only small improvement was observed in the rest of the steps with the inclusion of the less significant bivariate terms, such as $[x_2, x_3]$ and $[x_2, x_4]$. Table 6 summarizes the probability analysis results of the adaptive-sparse PCE with comparison with MCS, the 4th order PCE with full tensorized Gaussian

**Table 3** Probability analysis results for Franke's function

| | Adaptive-sparse PCE ($p = 9$) | MCS | $4N + 1$ UDR | FORM | SORM |
|---|---|---|---|---|---|
| Mean | 0.5604 | 0.5637 | 0.5615 | – | – |
| Std. dev. | 0.1737 | 0.1649 | 0.1619 | – | – |
| Skewness | 0.8400 | 0.7701 | 0.1488 | – | – |
| Kurtosis | 3.4826 | 3.3404 | 2.6452 | – | – |
| $R_1$ | 0.9012 | 0.8945 | 0.9221 | 0.8598 | 0.8717 |
| $\partial R_1/\partial \mu_1$ | 1.5475 | 1.5825[a] | – | – | – |
| $\partial R_1/\partial \mu_2$ | 1.5125 | 1.5475 | – | – | – |
| $R_2$ | 0.8041 | 0.8027 | 0.7961 | 0.7576 | 0.7723 |
| $\partial R_2/\partial \mu_1$ | 2.3925 | 2.3650 | – | – | – |
| $\partial R_2/\partial \mu_2$ | 2.3550 | 2.3475 | – | – | – |
| $R_3$ | 0.6484 | 0.6570 | 0.5992 | 0.6101 | 0.6214 |
| $\partial R_3/\partial \mu_1$ | 3.1950 | 3.1387 | – | – | – |
| $\partial R_3/\partial \mu_2$ | 3.4575 | 3.2150 | – | – | – |
| No. FE | 17 | 1,000,000 | 9 | 21/15/9 | 25/19/13 |

[a]MCS with finite difference (FD)

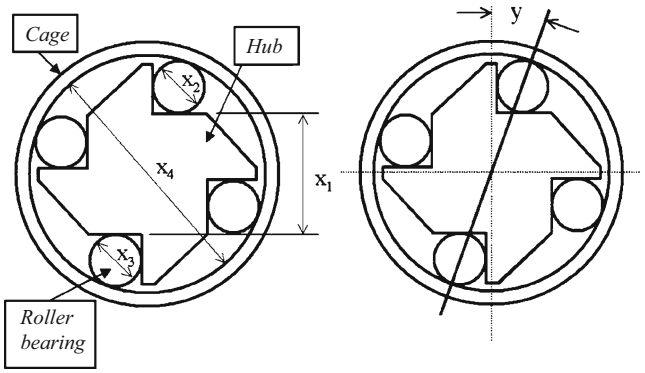


**Fig. 4** Fortini's clutch

quadrature ($M_1 = 5$), UDR, and FORM. Both the adaptive-sparse PCE and 4th order PCE produced more accurate results than the UDR and FORM at various reliability levels, including very low reliabilities (i.e., around $10^{-3}$) and very high reliabilities (i.e., around $1 - 10^{-3}$). Compared to the PCE, the adaptive-sparse PCE shows better performance with comparable accuracy and higher efficiency. The higher efficiency can be attributed to the use of the adaptive-sparse scheme to smartly select significant bivariate terms and the decomposition-based projection scheme to efficiently compute the PCE coefficients.

### 4.4 Burst margin of rotating disk: very low failure probability

Consider an annular disk of inner radius $R_i$, and outer radius $R_o$, as shown in Fig. 6. The disk rotates about its center at a constant angular velocity $w$. Three material parameters are the density $\delta$, ultimate tensile strength $S_u$, and material utilization factor $\alpha_u$. This example has been considered by Penmetsa and Grandhi (2003). The burst margin is defined as the margin of safety before an overstress condition occurs because the stress on the part is too large for the material to withstand. The failure is defined when the burst margin $M_b$ falls below the threshold value $M_c = 0.37437$. Thus, the performance function can be defined as follows:

$$g(\alpha_u, S_u, w, \delta, R_o, R_i) = M_c - M_b = 0.37473 - \left[\frac{3(385.82)(R_o - R_i)\alpha_u S_u}{\delta\left[\omega\frac{2\pi}{60}\right]^2\left(R_o^3 - R_i^3\right)}\right]^{1/2} \quad (37)$$

Statistical information of the random variables is listed in Table 7. In the adaptive-sparse PCE method, $M_1 = 4$, $M_2 = 8$, and $\varepsilon_1 = \varepsilon_2 = 0.01$. Using these parameter settings, the adaptive-sparse expansion scheme was converged with $p = 4$ and $q = 9$, as shown in Table 8. The convergence of the relative error of the failure probability is plotted in Fig. 7, which clearly shows the overall decreasing trend of the relative error with respect to $q$. The nine bivariate terms considered are listed as follows: $[x_1, x_4]$, $[x_1, x_3]$, $[x_2, x_3]$, $[x_1, x_5]$, $[x_2, x_5]$, $[x_2, x_4]$, $[x_2, x_6]$, $[x_3, x_5]$, and $[x_1, x_6]$, where $x_1$, $x_2$, $x_3$, $x_4$, $x_5$ and $x_6$ denote $\alpha_u$, $S_u$, $w$, $\delta$, $R_o$ and $R_i$, respectively. To investigate how a choice of the convergence parameters $\varepsilon_1$ and $\varepsilon_2$ affects the accuracy and efficiency of the adaptive-sparse PCE method, we conducted a parametric study with a three-level factorial design. In this study, each parameter was set at three levels-low (0.001), medium (0.010) and high (0.100), resulting in nine different parameter settings. The PCE orders, numbers of bivariate terms, reliability estimates and relative errors under these nine parameter settings are presented in Table 9, where L, M and H denote the low, medium and high levels, respectively. Three important remarks can be derived from the results. First of all, it is observed that the convergence parameter $\varepsilon_1$ of the outer loop in the adaptive-sparse scheme always has a significant effect on both the efficiency and accuracy, regardless of the levels of the convergence parameter $\varepsilon_2$ of the inner loop. More conservative criteria or smaller $\varepsilon_1$ values are likely to give higher accuracy but require more computational effort. It indicates that the optimum $\varepsilon_1$ may vary depending on the requirements on accuracy and efficiency. Secondly, the convergence parameter $\varepsilon_2$ of the inner loop does not significantly affect the accuracy. This observation is due to the fact that a very low order $p = 3$ is sufficient to accurately model the uncertainty in the performance function in this example. Indeed, an increase of the PCE order does not incur the improvement of accuracy as shown in Table 9. However, this observation cannot be generalized to other cases where a very high

**Table 4** Input random variables for the Fortini's clutch example

| Component | Distri. type | Mean (mm) | Std. dev. (mm) | Parameters for non-normal distributions |
|---|---|---|---|---|
| $x_1$ | Beta | 55.29 | 0.0793 | $\alpha_1 = \beta_1 = 5.0$[a] |
| $x_2$ | Normal | 22.86 | 0.0043 | – |
| $x_3$ | Normal | 22.86 | 0.0043 | – |
| $x_4$ | Rayleigh | 101.60 | 0.0793 | $\sigma_4 = 0.1211$[b] |

[a] $55.0269 \leq x_1 \leq 55.5531$; Jacobi polynomials
[b] $x_4 \geq 55.5531$; transformation to standard normal distribution

**Table 5** Adaptive-sparse process of the adaptive-sparse PCE for the Fortini's clutch example

| | PCE order ($p$) | No. of bivariate terms ($q$) | No. FE | $R^2$ | Reliability | Relative error (%) |
|---|---|---|---|---|---|---|
| Step 1 | 2 | 0 | 9 | 0.85268 | 0.000522 | 57.4919 |
| Step 2 | 2 | 1 | 22 | 0.85863 | 0.001270 | 3.4202 |
| Step 3 | 3 | 1 | 22 | 0.86631 | 0.001322 | 7.6547 |
| Step 4 | 4 | 1 | 22 | 0.86687 | 0.001411 | 14.9023 |
| Step 5 | 4 | 2 | 29 | 0.89659 | 0.001379 | 12.2964 |
| Step 6 | 4 | 3 | 36 | 0.85649 | 0.001371 | 11.6450 |

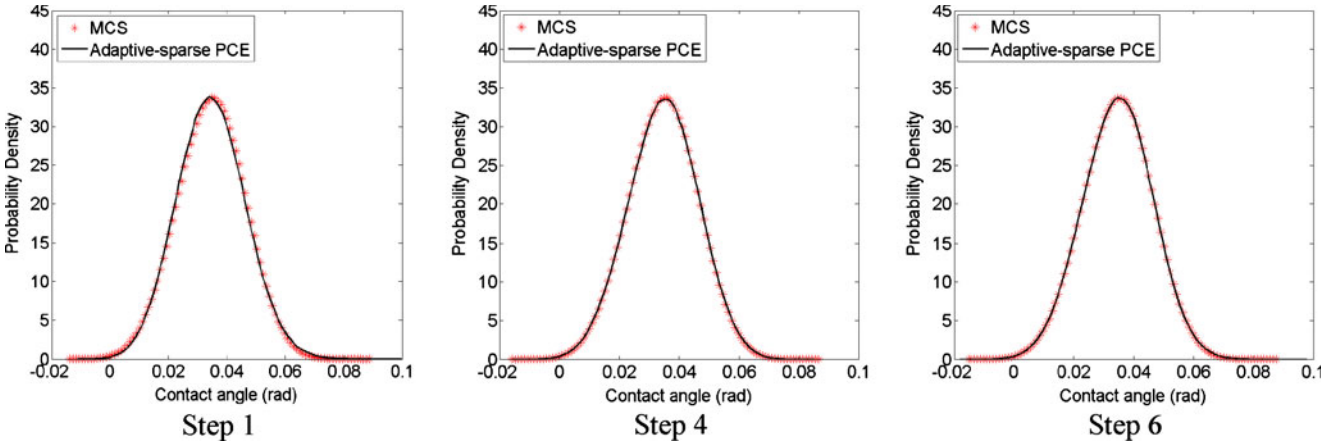


**Fig. 5** Evolution of PDF for the Fortini's clutch example

**Table 6** Probability analysis results for the Fortini's clutch example

| | Adaptive-sparse PCE ($p = 4$) | MCS | PCE ($p = 4$, Gauss quad) | $4N + 1$ UDR | FORM |
|---|---|---|---|---|---|
| Mean (rad) | 0.1219 | 0.1219 | 0.1219 | 0.1219 | – |
| Std. dev. (rad) | 0.0118 | 0.0117 | 0.0117 | 0.0116 | – |
| Skewness | −0.0514 | −0.0511 | −0.0563 | 0.0952 | – |
| Kurtosis | 2.8819 | 2.8805 | 2.8834 | 2.8775 | – |
| Pr($y < 5°$) | 0.001371 | 0.001228 | 0.001221 | 0.000486 | 0.002375 |
| Pr($y < 6°$) | 0.074769 | 0.073825 | 0.073761 | 0.066697 | 0.087707 |
| Pr($y < 7°$) | 0.503272 | 0.502903 | 0.503167 | 0.514469 | 0.520360 |
| Pr($y < 8°$) | 0.935685 | 0.936671 | 0.936288 | 0.933024 | 0.934922 |
| Pr($y < 9°$) | 0.999238 | 0.999233 | 0.999236 | 0.998696 | 0.999112 |
| Pr($5° < y < 9°$) | 0.997867 | 0.998005 | 0.998015 | 0.998210 | 0.996737 |
| No. FE | 36 | 1,000,000 | 625 | 17 | (100/25/10/15/25)[a] |

[a] 100 function evaluations for Pr($y < 5°$), 25 for Pr($y < 6°$), 10 for Pr($y < 7°$), 15 for Pr($y < 8°$), 25 for Pr($y < 9°$)

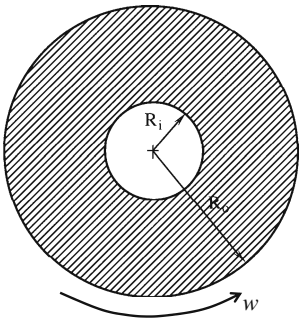


**Fig. 6** Rotating annular disk subject to angular velocity

PCE order and thus a very small $\varepsilon_2$ are required. Thirdly, we observe a negligible effect of interaction between the parameters $\varepsilon_1$ and $\varepsilon_2$ on the accuracy in reliability analysis. This observation can be attributed to the negligible effect of the parameter $\varepsilon_2$ on the accuracy as mentioned in the second remark. However, for engineering problems demanding a relatively high PCE order, we may observe a strong interaction effect between the two parameters $\varepsilon_1$ and $\varepsilon_2$ due to possible cancellation of errors produced by improper settings of these parameters. Table 10 summarizes the probability analysis results using the adaptive-sparse PCE, UDR, BDR (with the SMLS for response approximations and $M_1 = 4$, $M_2 = 8$), FORM and direct MCS. Regarding the failure probability estimation, the proposed adaptive-sparse PCE and BDR produced the most accurate solutions. The UDR overestimated the failure probability by 43%, whereas FORM underestimated the failure probability by 14%. In this problem, the UDR method outperforms the others in terms of efficiency, while the adaptive-sparse PCE method shows higher efficiency than the BDR and FORM. These results suggest that the adaptive-sparse PCE method achieves a good compromise between the UDR and BDR as commented in Remark 2.

**Table 7** Input random variables for the burst margin example

| Random inputs | Distri. type | Mean | Std. dev. | Parameters for non-normal distributions |
|---|---|---|---|---|
| $\alpha_u$ | Weibull | 0.9377 | 0.0459 | $\lambda_1 = 25.508, k_1 = 0.958$[a] |
| $S_u$, *ksi* | Normal | 220,000 | 5,000 | – |
| $w$, *rpm* | Normal | 21,000 | 1,000 | – |
| $\delta$, *lb/in*$^3$ | Uniform | 0.29 | 0.0058 | $a_4 = 0.28, b_4 = 0.30$[b] |
| $R_o$, *in* | Normal | 24 | 0.5 | – |
| $R_i$, *in* | Normal | 8 | 0.3 | – |

[a]Transformation to standard normal distribution
[b]Legendre polynomial

**Table 8** Adaptive-sparse process of the adaptive-sparse PCE for the burst margin example

| | PCE order ($p$) | No. of bivariate terms ($q$) | No. FE | $R^2$ | Failure probability | Relative error (%) |
|---|---|---|---|---|---|---|
| Step 1 | 2 | 0 | 25 | 0.92305 | 0.001376 | 32.308 |
| Step 2 | 2 | 1 | 47 | 0.91807 | 0.001392 | 33.846 |
| Step 3 | 3 | 1 | 47 | 0.98412 | 0.001600 | 53.846 |
| Step 4 | 4 | 1 | 47 | 0.99006 | 0.001581 | 52.019 |
| Step 5 | 4 | 2 | 54 | 0.99433 | 0.001352 | 30.000 |
| Step 6∼10 | – | – | – | – | – | – |
| Step 11 | 4 | 8 | 96 | 0.99673 | 0.001110 | 6.731 |
| Step 12 | 4 | 9 | 103 | 0.99654 | 0.001100 | 5.769 |

### 4.5 V6 gasoline engine power loss: bimodal PDF

This example is the V6 gasoline engine problem studied by Liu et al. (2006) and Lee and Chen (2007). The performance function considered in this example is the power loss due to the friction between the piston ring and the cylinder liner, oil consumption, blow-by, and liner wear rate. A ring/liner subassembly simulation model was used to compute the power loss. The simulation model has four input parameters, the ring surface roughness $x_1$, liner surface roughness $x_2$, liner Young's modulus $x_3$ and liner hardness $x_4$. Of the total four inputs, the first two, ring surface roughness $x_1$ and liner surface roughness $x_2$, were treated as random inputs following normal distributions with mean 4.0 and 6.119 μm, respectively, and with unit variance. The other two inputs, liner Young's modulus $x_3$ and liner hardness $x_4$, were treated as deterministic inputs fixed at 80 GPa and 240 BHV, respectively. It has been shown in Lee and Chen (2007) that the

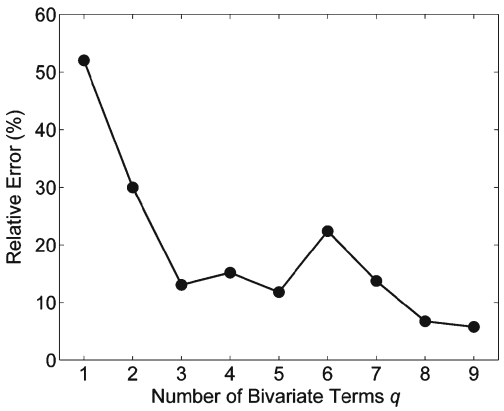


**Fig. 7** Convergence of failure probability with respect to the number of bivariate terms

**Table 9** Results of adaptive-sparse scheme and reliability analysis in parametric study

| $\varepsilon_1$ | $\varepsilon_2$ | $p$ | $q$ | Pr($g > 0$) | Rel. error (%) | No. FE |
|---|---|---|---|---|---|---|
| L (0.001) | L (0.001) | 7 | 15 | 0.001063 | 2.212 | 145 |
| | M (0.01) | 4 | 15 | 0.001070 | 2.885 | 145 |
| | H (0.1) | 3 | 14 | 0.001067 | 2.596 | 138 |
| M (0.01) | L (0.001) | 7 | 9 | 0.001110 | 6.731 | 103 |
| | M (0.01) | 4 | 9 | 0.001100 | 5.769 | 103 |
| | H (0.1) | 3 | 9 | 0.001116 | 7.308 | 103 |
| H (0.1) | L (0.001) | 7 | 4 | 0.001216 | 16.923 | 68 |
| | M (0.01) | 4 | 4 | 0.001198 | 15.192 | 68 |
| | H (0.1) | 3 | 3 | 0.001245 | 19.712 | 61 |

power loss has a bimodal PDF. To predict the bimodal PDF, the adaptive-sparse PCE used $M_1 = 20$ and $M_2 = 20$. As shown in Table 11, the adaptive-sparse expansion scheme was converged with $p = 25$ and $q = 1$. Figure 8 shows the PDF approximations by the 16th, 20th and 25th order PCEs with full tensorized Gaussian quadrature ($M_1 = 17$ for $p = 16$, $M_1 = 21$ for $p = 20$, and $M_1 = 26$ for $p = 25$), UDR and adaptive-sparse PCE. Both the adaptive-sparse PCE and 20th order PCE with Gaussian quadrature produced accurate approximations for the left peak and tail regions of the PDF. The 16th order PCE could not accurately approximate this bimodal PDF (see Fig. 8a) while the 25th order PCE gave the most accurate solution. As shown in Fig. 8b, the UDR failed to represent the irregular shape of this PDF due to the same reasons explained in Section 4.2. The comparison results in Table 12 suggest that the adaptive-sparse PCE method is more accurate than the UDR method, particularly for system responses with strong bivariate interactions. The error in the probability estimation by FORM is due to the nonlinearity of the power loss function. The computational cost by the adaptive-sparse PCE method is much lower than that by the conventional PCE method with full tensorized Gaussian quadrature.

**Table 10** Probability analysis results for burst margin example

| | Adaptive-sparse PCE ($p = 4$) | MCS | $4N + 1$ UDR | BDR | FORM |
|---|---|---|---|---|---|
| Mean | 0.0787 | 0.0787 | 0.0787 | 0.0787 | – |
| Std. dev. | 0.0268 | 0.0268 | 0.0267 | 0.0268 | – |
| Skewness | 0.1619 | 0.1734 | 0.0830 | 0.1787 | – |
| Kurtosis | 3.1523 | 3.1403 | 3.1335 | 3.1514 | – |
| Pr($g > 0$) | 0.00110 | 0.00104 | 0.00149 | 0.00107 | 0.00089 |
| No. FE | 103 | 1,000,000 | 25 | 145 | 131 |

**Table 11** Adaptive-sparse process of the adaptive-sparse PCE for the V6 engine example

| | PCE order ($p$) | No. of bivariate terms ($q$) | No. FE | $R^2$ | Reliability | Relative error (%) |
|---|---|---|---|---|---|---|
| Step 1 | 2 | 0 | 41 | 0.98842 | 0.00687 | 26.987 |
| Step 2 | 2 | 1 | 61 | 0.98810 | 0.00717 | 32.532 |
| Step 3 | 3 | 1 | 61 | 0.97922 | 0.00468 | 13.494 |
| Step 4∼23 | – | – | – | – | – | – |
| Step 24 | 24 | 1 | 61 | 0.98197 | 0.00547 | 1.109 |
| Step 25 | 25 | 1 | 61 | 0.98273 | 0.00547 | 1.109 |

### 4.6 Side-impact crash problem: nonlinear correlation

Vehicle side-impact responses (Youn et al. 2004) are considered for system performances with statistical nonlinear correlation modeled by a copula theory (Roser 1999; Noh et al. 2008). The properties of the design and random variables are shown in Table 13. This example considered the velocity of a front door at B-pillar. The failure is defined when the velocity exceeds the threshold value 15.7. Thus, the system performance can be expressed as

$$g(\mathbf{x}) = \left(16.45 - 0.489x_1x_4 - 0.843x_2x_3 + 0.0432x_5x_6 - 0.0556x_5x_7 - 0.000786x_7^2\right) - 15.7 \quad (38)$$

In the study, the random variables $x_6$ and $x_7$ with the maximum variation were assumed to have a statistical nonlinear correlation described by a Clayton copula, as shown in Fig. 9a. The rank correlation coefficient was used to quantify the nonlinear correlation. In this case, we assumed the rank correlation coefficient Kendall's $\tau$ to be 0.75 and the corresponding copula parameter to be 6.0. As discussed in Section 3.3, the Rosenblatt transformation is required to transform correlated input variables into uncorrelated standard normal variables. Using $M_1 = 4$ and $M_2 = 8$, the adaptive-sparse expansion scheme was converged with $p = 3$ and $q = 2$ and one of the bivariate terms considered was [$x_6$, $x_7$], which were nonlinearly correlated. To illustrate the effect of statistical nonlinear correlation on the system response, the PDFs for both correlated and uncorrelated cases are shown in Fig. 9b. It shows that the nonlinear correlation affects the PDF of the system performance significantly and that the adaptive-sparse PCE method accurately predicted the peak and tail regions of the PDF. Quantitative results are summarized in Table 14. To further study the effects of different correlation coefficients on the reliability estimation, we plotted in Fig. 10 the reliabilities for increasing values of Kendall's $\tau$. As shown in the figure, the correlation

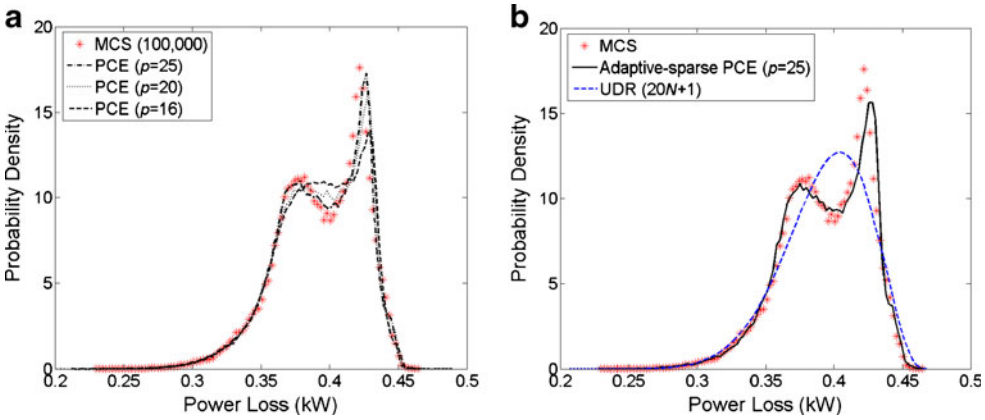


**Fig. 8** PDF approximations by the PCEs (**a**), adaptive-sparse PCE and UDR (**b**) for the V6 engine example

**Table 12** Probability analysis results for the V6 engine example

| | Adaptive-sparse PCE ($p = 25$) | MCS | PCE ($p = 20$, Gauss quad) | $20N + 1$ UDR | FORM |
|---|---|---|---|---|---|
| Mean (kW) | 0.3935 | 0.3935 | 0.3934 | 0.3935 | – |
| Std. dev. (kW) | 0.0315 | 0.0310 | 0.0311 | 0.0314 | – |
| Skewness | −0.5527 | −0.5883 | −0.5735 | −0.5393 | – |
| Kurtosis | 3.0249 | 3.0828 | 3.0599 | 3.0974 | – |
| Pr(PL < 0.3) | 0.0056 | 0.0054 | 0.0054 | 0.0048 | 0.0057 |
| No. FE | 61 | 100,000 | 441 | 41 | 15 |

**Table 13** Input random variables for the side impact example

| Random input | Distri. type | Mean | Std. dev. | Lower bound | Upper bound | Mode |
|---|---|---|---|---|---|---|
| $x_1$ | Beta | 1.500 | 0.050 | 1.000 | 1.800 | – |
| $x_2$ | Uniform | – | – | 0.850 | 1.150 | – |
| $x_3$ | Uniform | – | – | 0.699 | 0.999 | – |
| $x_4$ | Uniform | – | – | 0.850 | 1.150 | – |
| $x_5$ | Triangular | – | – | 0.327 | 0.363 | 0.345 |
| $x_6$ | Normal | 0 | 10.000 | – | – | – |
| $x_7$ | Normal | 0 | 10.000 | – | – | – |

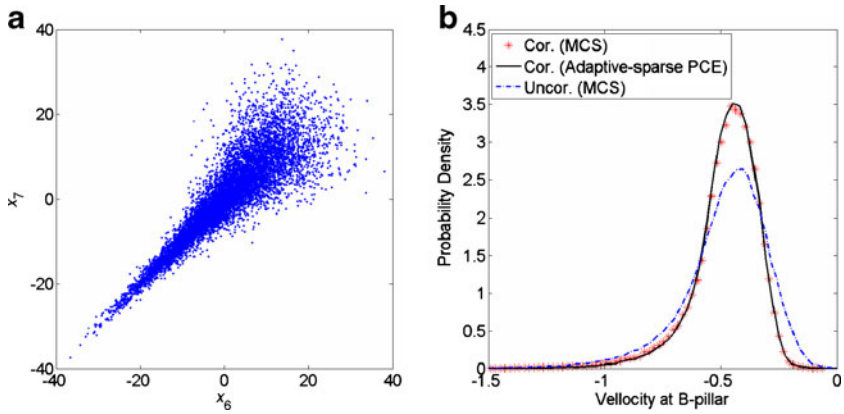


**Fig. 9** Scatter plot of input variables $x_6$ and $x_7$ (**a**), and PDF results (**b**)

**Table 14** Probability analysis results for the side impact example ($\tau = 0.75$)

| | Adaptive-sparse PCE ($p = 3$) | MCS |
|---|---|---|
| Mean | −0.4766 | −0.4813 |
| Std. dev. | 0.1408 | 0.1520 |
| Skewness | −1.7109 | −1.7402 |
| Kurtosis | 10.2690 | 9.2106 |
| Pr($g < 0$) | 0.9496 | 0.9437 |
| No. FE | 64 | 1,000,000 |

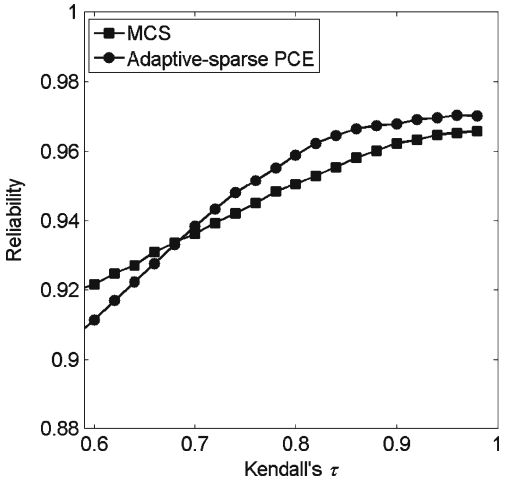


**Fig. 10** Reliabilities for increasing values of Kendall's $\tau$

coefficients significantly affect the reliabilities and the adaptive-sparse PCE maintains consistent accuracy within ±0.01 at all reliability levels.

## 4.7 Lower control A-arm: RBRDO against a fatigue failure

Vehicle suspension systems experience intense loading conditions throughout their service lives. Control arms act as the backbone of the suspension system, through which the majority of these loads are transmitted (Youn et al. 2007b). Therefore, it is crucial that control arms be highly reliable while its mass is minimized. The HMMWV lower control-arm was modeled with plane stress elements using 54,666 nodes, 53,589 elements, and 327,961 DOFs, where all welds were modeled using rigid beam elements. HyperWorks 8.0 was used for FE modeling and design parameterization. The loading and boundary conditions are shown in Fig. 11a. The loading was applied at the ball-joint (point D) in three directions, and the boundary conditions were applied to simulate the bushing joints (points A and B) and the joint with a shock absorber and spring assemble (point C). This lower control-arm model was used for RBRDO using the adaptive-sparse PCE method.

### *4.7.1 RBRDO formulation*

From a worst-case scenario analysis, 91 constraints ($G_1$ to $G_{91}$) were defined in several critical regions using the von Mises stress, as shown in Fig. 12. With 91 stress constraints, the RBRDO is formulated as

$$\begin{aligned} &\text{Minimize} \quad Q = \mu_m + \sigma_m \\ &\text{Subject to} \quad R_i = \Pr\left(G_i(\mathbf{x};\mathbf{d}) = \frac{s_i(\mathbf{x};\mathbf{d})}{s_y} - 1 \le 0\right) \\ &\qquad\qquad \ge \Phi\left(\beta_i^t\right) = R_i^t, \ i = 1, \cdots, 91 \\ &\qquad \mathbf{d}^{\mathbf{L}} \le \mathbf{d} \le \mathbf{d}^{\mathbf{U}} \end{aligned} \tag{39}$$

where, the objective function $Q$ is the summation of the mean $\mu_m$ and standard deviation $\sigma_m$ of the mass; $\mathbf{x}$ is the random vector; $\mathbf{d} = \boldsymbol{\mu}(\mathbf{x})$ is the design vector; $s_i$ is the von Mises stress of the $i^{th}$ constraint; $s_y$ is the yield stress and was set to 60.9 ksi for any constraint; $R_i^t$ is the target reliability level and was set to 99.87% for any constraint, which corresponds to a target reliability index $\beta_i^t = 3.0$. The seven design variables are the thicknesses of the seven major components of the control arm, as shown in Fig. 11b. Three load variables (not design variables) are considered as random

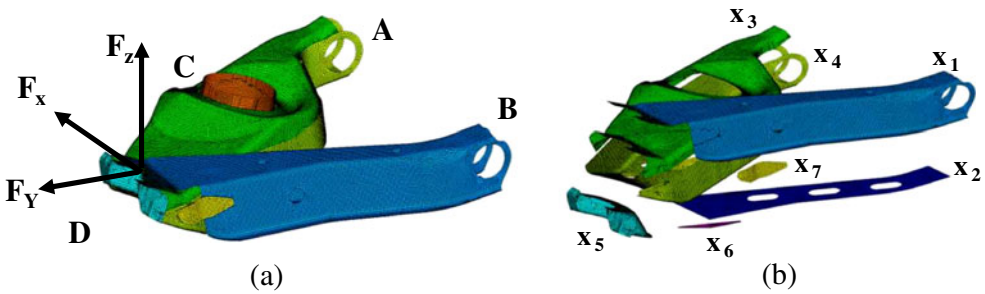


**Fig. 11** Three random load variables (**a**) and seven design variables (**b**)

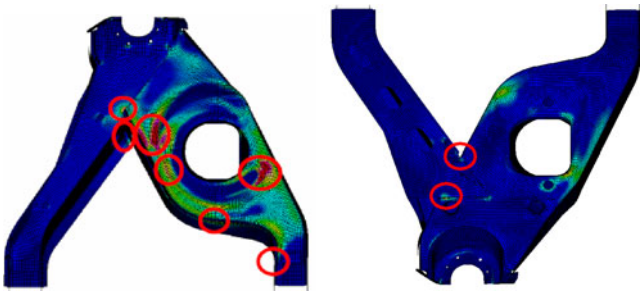

**Fig. 12** Ninety-one critical constraints of the lower control A-arm model

**Table 15** Random force variables for the lower control A-arm model

| Random variable | Distri. type | Mean | Std. dev. |
|---|---|---|---|
| $F_X$ | Normal | 1,900 | 95 |
| $F_Y$ | Normal | 95 | 4.75 |
| $F_Z$ | Normal | 950 | 47.5 |

**Table 16** Design variables for the lower control A-arm model

| Design variable | Distri. type | Lower bound | Initial des. | Upper bound | Std. dev. |
|---|---|---|---|---|---|
| $x_1$ | Normal | 0.100 | 0.120 | 0.500 | 0.006 |
| $x_2$ | Normal | 0.100 | 0.120 | 0.500 | 0.006 |
| $x_3$ | Normal | 0.100 | 0.180 | 0.500 | 0.009 |
| $x_4$ | Normal | 0.100 | 0.135 | 0.500 | 0.007 |
| $x_5$ | Normal | 0.150 | 0.250 | 0.500 | 0.013 |
| $x_6$ | Normal | 0.100 | 0.180 | 0.500 | 0.009 |
| $x_7$ | Normal | 0.100 | 0.135 | 0.500 | 0.007 |

noisy variables. The statistical information of these random and design variables is summarized in Tables 15 and 16 respectively.

### *4.7.2 Optimization results*

The adaptive-sparse PCE method with $4N + 1(= 41)$ FE analyses was carried out to evaluate the quality function, 91 reliabilities, and their sensitivities at any design iteration, without considering the bivariate polynomial basis functions. The sensitivities of the quality function and reliabilities with respect to the seven design variable were computed by using a finite difference method (FDM) at each design Iteration. The perturbed values of the quality function and reliabilities were estimated based on approximate stochastic response surfaces (PCE) with perturbed design variables, without requiring gradients of the original mass or stress functions. A perturbation size of 0.1% is employed in this study.

The design optimization problem was solved using a gradient-based optimization technique (e.g., sequential quadratic optimization). The histories of the design parameters, objective function, and reliabilities for significant constraints $G_6$, $G_{80}$ and $G_{87}$ are shown in Table 17. At the initial design, the constraints $G_6$ and $G_{80}$ severely violated the reliability requirement. After seven design iterations, the optimum design was found where all the reliability requirements were satisfied. Overall, the adaptive-sparse PCE method required 287 FE simulations for RBRDO. After the optimization, the direct MCS with 5,000 random samples was employed to verify the reliability results at the optimum design. The reliabilities of constraints $G_6$, $G_{80}$ and $G_{87}$ were estimated by the MCS as 99.71%, 99.88%, and 99.84%, respectively, and all the other constraints were confirmed with 100% reliabilities. The stress contours at the

**Table 17** Design history of the lower control A-arm model

| Iter. | Design variables | | | | | | | $R_6$ | $R_{80}$ | $R_{87}$ | Obj. |
|---|---|---|---|---|---|---|---|---|---|---|---|
| | $x_1$ | $x_2$ | $x_3$ | $x_4$ | $x_5$ | $x_6$ | $x_7$ | | | | |
| 0 | 0.120 | 0.120 | 0.180 | 0.135 | 0.250 | 0.180 | 0.135 | 0.3235 | 0.0050 | 1.0000 | 31.473 |
| 1 | 0.100 | 0.142 | 0.150 | 0.164 | 0.150 | 0.500 | 0.100 | 0.9989 | 0.9970 | 0.9620 | 32.044 |
| 2 | 0.100 | 0.140 | 0.169 | 0.161 | 0.150 | 0.500 | 0.325 | 0.9988 | 0.9982 | 0.9998 | 32.875 |
| 3 | 0.100 | 0.140 | 0.160 | 0.162 | 0.150 | 0.500 | 0.336 | 0.9982 | 0.9986 | 0.9963 | 32.513 |
| 4 | 0.100 | 0.140 | 0.164 | 0.164 | 0.150 | 0.500 | 0.228 | 0.9988 | 0.9989 | 0.9991 | 32.763 |
| 5 | 0.100 | 0.140 | 0.162 | 0.164 | 0.150 | 0.500 | 0.224 | 0.9986 | 0.9984 | 0.9982 | 32.607 |
| 6 | 0.100 | 0.140 | 0.163 | 0.164 | 0.150 | 0.500 | 0.211 | 0.9985 | 0.9988 | 0.9991 | 32.697 |
| 7 | 0.100 | 0.140 | 0.164 | 0.164 | 0.150 | 0.500 | 0.210 | 0.9987 | 0.9989 | 0.9991 | 32.717 |
| Opt | 0.100 | 0.140 | 0.164 | 0.164 | 0.150 | 0.500 | 0.210 | 0.9987 | 0.9989 | 0.9991 | 32.717 |

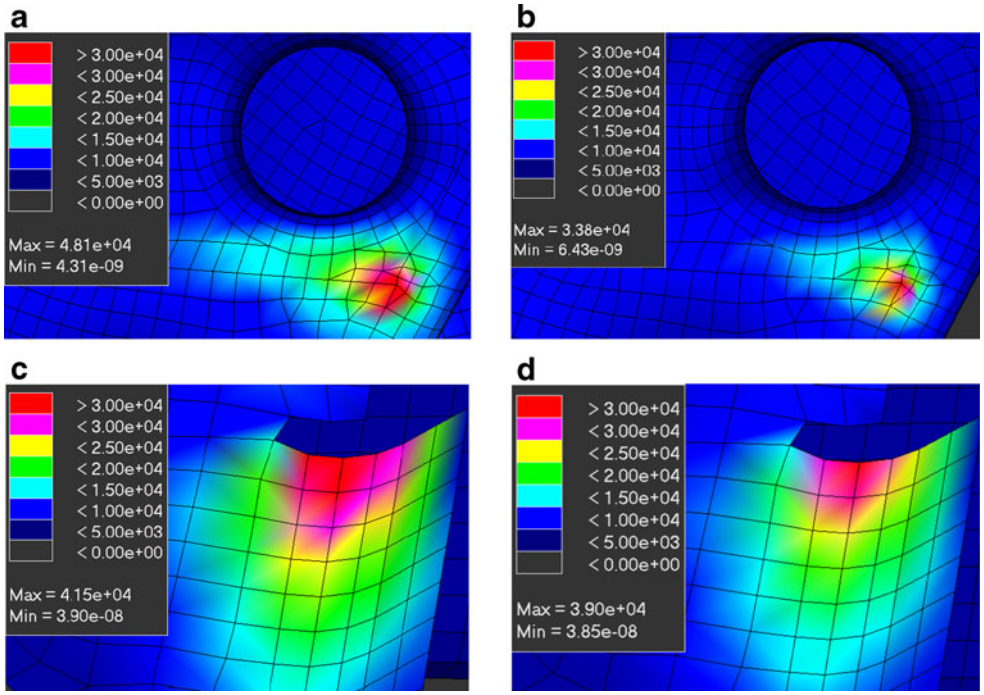


**Fig. 13** Stress comparisons of initial and optimum design: **a** $G_6$ at initial design, **b** $G_6$ at optimum design, **c** $G_{80}$ at initial design, **d** $G_{80}$ at optimum design

initial and optimum designs for constraints $G_6$ and $G_{80}$ are shown in Fig. 13. It can be seen in both constraints that the high stress areas are greatly reduced by the RBRDO process.

## 5 Conclusion

The adaptive-sparse PCE method was proposed for efficient structural reliability analysis involving high nonlinearity or large dimension. The adaptive-sparse PCE method combines four ideas and methods: (1) an adaptive-sparse scheme to determine the number ($q$) of the most significant bivariate terms and PCE order ($p$) in the PCE model; (2) an efficient decomposition-based projection method using the SMLS method; (3) the integration of the copula system to handle nonlinear correlation of input random variables, and (4) the systematic error decomposition analysis in the proposed method. It was found in many examples that the adaptive-sparse scheme and decomposition-based projection method achieves greater accuracy and efficiency than other probability/reliability methods, including FORM/SORM and moment-based reliability methods. This high accuracy can be attributed to the consideration of significant bivariate response components and the accurate integration scheme by the SMLS method. The adaptive-sparse PCE method can also approximate a multi-modal PDF as shown in Section 4.5. Moreover, the proposed method is stable, unlike other probability/reliability methods, since it does not require a distribution generation system. Future works will focus on the integration of the adaptive-sparse PCE method with system reliability analysis and design optimization.

**Acknowledgments** The authors would like to acknowledge that this research is partially supported by US National Science Foundation (NSF) under Grant No. GOALI-0729424, U.S. Army TARDEC by the STAS contract (TCN-05122), and by General Motors under Grant No. TCS02723.

## Appendix

The derivation of the error decomposition

Error source I: Truncation

$$\varepsilon_P^2 = \int_\Gamma \left[g - w_{UB}^p\right]^2 f(\mathbf{x}) d\mathbf{x}$$

$$= \int_\Gamma \left[ \begin{array}{l} \sum_k \sum_{j>p} s_j^k \cdot \Phi_j(\zeta_k) \\ + \sum_{[x_k,x_l]\notin \mathbf{B}} \sum_{j_1+j_2\le p} s_{j_1,j_2}^{k,l} \cdot \Phi_{j_1,j_2}(\zeta_k,\zeta_l) \\ + \sum_{k<l} \sum_{j_1+j_2>p} s_{j_1,j_2}^{k,l} \cdot \Phi_{j_1,j_2}(\zeta_k,\zeta_l) \\ + \sum_{k<l<m} \sum_{j_1,j_2,j_3\ge 1} s_{j_1,j_2,j_3}^{k,l,m} \\ \cdot \Phi_{j_1,j_2,j_3}(\zeta_k,\zeta_l,\zeta_m) + \cdots \end{array} \right]^2 f(\mathbf{x}) d\mathbf{x}$$

Error source II: Bivariate decomposition

$$\varepsilon_B^2 = \int_\Gamma \left[w_{UB}^p - w_U^p\right]^2 f(\mathbf{x})d\mathbf{x}$$
$$= \int_\Gamma \left[\sum_{[x_k,x_l]\in\mathbf{B}} \sum_{j_1+j_2\le p} \left(s_{j_1,j_2}^{k,l} - \hat{s}_{j_1,j_2}^{k,l}\right)\Phi_{j_1,j_2}(\zeta_k,\zeta_l)\right]^2 f(\mathbf{x})d\mathbf{x}$$
$$= \int_\Gamma \left[\sum_{[x_k,x_l]\in\mathbf{B}} \sum_{j_1+j_2\le p} \frac{E\left[\left(g(\mathbf{x}) - g\left(x_k,x_l,\boldsymbol{\mu}^{k,l}\right)\right)\cdot\Phi_{j_1,j_2}(\zeta_k,\zeta_l)\right]}{E\left[\Phi_{j_1,j_2}^2(\zeta_k,\zeta_l)\right]}\cdot\Phi_{j_1,j_2}(\zeta_k,\zeta_l)\right]^2 f(\mathbf{x})d\mathbf{x}$$

where

$$E\left[\left(g(\mathbf{x}) - g\left(x_k,x_l,\boldsymbol{\mu}^{k,l}\right)\right)\Phi_{j_1,j_2}(\zeta_k,\zeta_l)\right]$$
$$= \frac{1}{2!1!1!}\sum_{i\ne k,l}\frac{\partial^4 g}{\partial x_i^2\partial x_k\partial x_l}(\boldsymbol{\mu})\cdot E\left[(x_i-\mu_i)^2(x_k-\mu_k)(x_l-\mu_l)\Phi_{j_1,j_2}(\zeta_k,\zeta_l)\right]+\cdots$$

Error source III: Univariate decomposition

$$\varepsilon_U^2 = \int_\Gamma \left[w_U^p - w_I^p\right]^2 f(\mathbf{x})d\mathbf{x} = \int_\Gamma \left[\sum_{k=1}^N\sum_{j=1}^p \left(s_j^k - \hat{s}_j^k\right)\Phi_j(\zeta_k)\right]^2 f(\mathbf{x})\,d\mathbf{x}$$
$$= \int_\Gamma \left[\sum_{k=1}^N\sum_{j=1}^p \frac{E\left[\left(g(\mathbf{x}) - g\left(x_k,\boldsymbol{\mu}^k\right)\right)\Phi_j(\zeta_k)\right]}{E\left[\Phi_j^2(\zeta_k)\right]}\cdot\Phi_j(\zeta_k)\right]^2 f(\mathbf{x})d\mathbf{x}$$

where

$$E\left[\left(g(\mathbf{x}) - g(x_k,\boldsymbol{\mu}^k)\right)\Phi_j(\zeta_k)\right] = \frac{1}{2!1!}\sum_{i\ne k}\frac{\partial^3 g}{\partial x_i^2\partial x_k}(\boldsymbol{\mu})E\left[(x_i-\mu_i)^2(x_k-\mu_k)\Phi_j(\zeta_k)\right]+\cdots$$

Error source IV: Aliasing error

$$\varepsilon_I^2 = \int_\Gamma \left[w_I^p - w^p\right]^2 f(\mathbf{x})d\mathbf{x}$$
$$= \int_\Gamma \left[\sum_{k=1}^N\sum_{j=1}^p \left(\hat{s}_j^k - \hat{\hat{s}}_j^k\right)\Phi_j(\zeta_k) + \sum_{[x_k,x_l]\in\mathbf{B}}\sum_{j_1+j_2\le p}\left(\hat{s}_{j_1,j_2}^{k,l} - \hat{\hat{s}}_{j_1,j_2}^{k,l}\right)\Phi_{j_1,j_2}(\zeta_k,\zeta_l)\right]^2 f(\mathbf{x})d\mathbf{x}$$
$$= \int_\Gamma \left[\begin{array}{l}\displaystyle\sum_{k=1}^N\sum_{j=1}^p \frac{\left(E-\hat{E}\right)\left[g\left(x_k,\boldsymbol{\mu}^k\right)\Phi_j(\zeta_k)\right]}{E\left[\Phi_j^2(\zeta_k)\right]}\cdot\Phi_j(\zeta_k) \\ \quad\displaystyle+\sum_{[x_k,x_l]\in\mathbf{B}}\sum_{j_1+j_2\le p}\frac{\left(E-\hat{E}\right)\left[g(x_k,x_l,\boldsymbol{\mu}^{k,l})\cdot\Phi_{j_1,j_2}(\zeta_k,\zeta_l)\right]}{E\left[\Phi_{j_1,j_2}^2(\zeta_k,\zeta_l)\right]}\cdot\Phi_{j_1,j_2}(\zeta_k,\zeta_l)\end{array}\right]^2 f(\mathbf{x})d\mathbf{x}$$

where $\hat{E}(\cdot)$ denotes the approximate expectation by using the SMLS and Gaussian quadrature integration.

## References


Au SK, Beck JL (2001) Estimation of small failure probabilities in high dimensions by subset simulation. Probab Eng Mech 16(4):263−277

Bieri M, Schwab C (2009) Sparse high order FEM for elliptic sPDEs. Comput Methods Appl Mech Eng 198:1149−1170

Blatman G, Sudret B (2008) Sparse polynomial chaos expansions and adaptive stochastic finite elements using a regression approach. Comptes Rendus Mécanique 336(6):518−523

Breitung K (1984) Asymptotic approximations for multinormal integrals. J Eng Mech Div ASCE 110(3):357−366

Cameron RH, Martin WT (1947) The orthogonal development of nonlinear functionals in series of Fourier−Hermite functionals. Ann Math 48:385−392

Choi S, Grandhi RV, Canfield RA (2004a) Structural reliability under non-Gaussian stochastic behavior. Comput Struct 82:1113−1121

Choi S, Grandhi RV, Canfield RA, Pettit CL (2004b) Polynomial chaos expansion with latin hypercube sampling for estimating response variability. AIAA J 42(n6):1191−1198

Creveling CM (1997) Tolerance design: a handbook for developing optimal specification. Addison-Wesley, Cambridge

Field RV (2002) Numerical methods to estimate the coefficients of the polynomial chaos expansion. In: Proceedings of the 15th ASCE engineering mechanics conference

Foo J, Karniadakis GE (2010) Multi-element probabilistic collocation method in high dimensions. J Comput Phys 229:1536−1557

Foo J, Wan X, Karniadakis GE (2008) The multi-element probabilistic collocation method (ME-PCM): error analysis and applications. J Comput Phys 227:9572−9595

Franke R (1979) A critical comparison of some methods for interpolation of scattered data. Naval Postgraduate School Technical Report, NPS-53-79-003

Fu G, Moses F (1988) Importance sampling in structural system reliability. In: Proceedings of ASCE joint specialty conference on probabilistic methods. Blacksburg, Virginia, United States, pp 340−343

Gerstner T, Griebel M (1998) Numerical integration using sparse grids. Numer Algorithms 18(3):209−232

Gerstner T, Griebel M (2003) Dimension-adaptive tensor-product quadrature. Computing 71(1):65−87

Ghanem RG, Spanos PD (1991) Stochastic finite elements: a spectral approach. Springer, New York

Han J, Kamber M (2000) Data mining: concepts and techniques (the Morgan Kaufmann Series in data management systems). Morgan Kaufmann

Hasofer AM, Lind NC (1974) Exact and invariant second-moment code format. J Eng Mech Div ASCE 100:111−121

Kohavi R (1995) A study of cross-validation and bootstrap for accuracy estimation and model selection. In: Proceedings of the international joint conference on artificial intelligence—IJCAI'95'

Le Maître OP, Knio OM, Najm HN, Ghanem RG (2001) A stochastic projection method for fluid flow—I. Basic formulation. J Comput Phys 173:481−511

Le Maître OP, Reagan M, Najm HN, Ghanem RG, Knio OM (2002) A stochastic projection method for fluid flow—II. Random process. J Comput Phys 181:9−44

Le Maitre O, Najm H, Ghanem R, Knio O (2004) Multi-resolution analysis of Wiener-type uncertainty propagation schemes. J Comput Phys 197:502−531

Lee SH, Chen W (2007) A comparative study of uncertainty propagation methods for black-box-type problems. Struct Multidiscipl Optim. doi:10.1007/s00158-008-0234-7

Lee SH, Kwak BM (2005) Response surface augmented moment method for efficient reliability analysis. Struct Saf 28:261−272

Lee I, Choi KK, Du L, Gorsich D (2008) Dimension reduction method for reliability-based robust design optimization. Comput Struct 86(13−14):1550−1562

Liu H, Chen W, Kokkolaras M, Papalambros PY, Kim HM (2006) Probabilistic analytical target cascading: a moment matching formulation for multilevel optimization under uncertainty. J Mech Des 128(4):991−1000

Ma X, Zabaras N (2009) An adaptive hierarchical sparse grid collocation algorithm for the solution of stochastic differential equations. J Comput Phys 228:3084−3113

Noh Y, Choi KK, Du L (2008) Selection of copula to generate input joint CDF for RBDO. In: ASME international design engineering technical conference & computers and information in engineering conference, IDETC2008-49494, Brooklyn, New York, United States, 3−6 August 2008

Noh Y, Choi KK, Du L (2009) Reliability-based design optimization of problems with correlated input variables using a Gaussian Copula. Struct Multidiscipl Optim 38(1):1−16

Paffrath M, Wever U (2007) Adapted polynomial chaos expansion for failure detection. J Comput Phys 226:263−281

Penmetsa R, Grandhi R (2003) Adaptation of fast Fourier transformations to estimate structural failure probability. Finite Elem Anal Des 39:473−485

Rahman S (2006) A dimensional decomposition method for stochastic fracture mechanics. Eng Fract Mech 73(15):2093−2109

Rahman S (2009) Stochastic sensitivity analysis by dimensional decomposition and score functions. Probab Eng Mech 24(3):278−287

Rahman S, Xu H (2004) A univariate dimension-reduction method for multi-dimensional integration in stochastic mechanics. Probab Eng Mech 19:393−408

Rosenblatt M (1952) Remarks on a multivariate transformation. Ann Math Stat 23:470−472

Roser BN (1999) An introduction to copulas. Springer, New York

Rubinstein RY (1981) Simulation and the Monte Carlo method. Wiley, New York

Smolyak SA (1963) Quadrature and interpolation formulas for tensor products of certain classes of functions. Sov Math Dokl 4:240−243

Sudret B, Der Kiureghian A (2002) Comparison of finite element reliability methods. Probab Eng Mech 17:337−348

Todor RA, Schwab C (2007) Convergence rates for sparse chaos approximations of elliptic problems with stochastic coefficients. IMA J Numer Anal 27:232−261

Tvedt L (1984) Two second-order approximations to the failure probability. Section on structural reliability. A/S Vertas Research, Hovik

Wan X, Karniadakis GE (2005) An adaptive multi-element generalized polynomial chaos method for stochastic differential equations. J Comput Phys 209(2):617−642

Wan X, Karniadakis GE (2006) Multi-element generalized polynomial chaos for arbitrary probability measures. SIAM J Sci Comput 28:901−928

Wang LP, Grandhi RV (1996) Safety index calculation using intervening variables for structural reliability. Comput Struct 59(6):1139−1148

Wiener N (1938) The homogeneous chaos. Am J Math 60:897−936

Wu CC, Chen Z, Tang GR (1998) Component tolerance design for minimum quality loss and manufacturing cost. Comput Ind 35:223−232

Xiu D (2009) Fast numerical methods for stochastic computations: a review. Communications in Computational Physics 5:242−272

Xiu D, Karniadakis GE (2003) The Wiener−Askey polynomial chaos for stochastic differential equations. SIAM J Sci Comput 187:137−167

Xu H, Rahman S (2004) A generalized dimension-reduction method for multi-dimensional integration in stochastic mechanics. Int J Numer Methods Eng 61:1992−2019

Youn BD, Choi KK (2004a) An investigation of nonlinearity of reliability-based design optimization approaches. J Mech Des 126(3):403−411

Youn BD, Choi KK (2004b) A new response surface methodology for reliability based design optimization. Comput Struct 82:241−256

Youn BD, Choi KK, Gu L, Yang RJ (2004) Reliability-based design optimization for crashworthiness of side impact. J Struct Multidiscipl Optim 26(3−4):272−283

Youn BD, Zhimin X, Wang P (2007a) Eigenvector dimension reduction (EDR) method for sensitivity-free probability analysis. Struct Multidiscipl Optim 37:13−28

Youn BD, Zhimin X, Wang P (2007b) Reliability-based robust design optimization using the eigenvector dimension reduction (EDR) method. Struct Multidiscipl Optim 37:475−492

Zhao YG, Ono T (2001) Moment methods for structural reliability. Struct Saf 23(1):47−75